Theory of the Reconstruction of the (111) Surfaces of Si and Ge

Yoshifumi Sakamoto

DISSERTATION IN PHYSICS

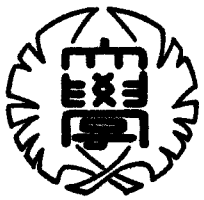

THE OSAKA UNIVERSITY

GRADUATE SCHOOL OF SCIENCE

TOYONAKA, OSAKA

Theory of the Reconstruction of the (111) Surfaces of Si and Ge

by
Yoshifumi Sakamoto

synopsis

Two lattice gas models which describe well the surface reconstruction of Ge(111) and Si(111), respectively, both below and above the transition are proposed. For the Ge(111) case, a lattice gas model on a triangular net with up to the sixth neighbour pairwise interaction is proposed. Monte Carlo calculations of phase diagrams and diffuse scatterings of electron in the high-temperature (1×1) phases within the kinematical approximation are presented. The phase transition from the ordered state to the (1×1) one is shown to be of the first kind. It is also shown in the calculation of diffuse scatterings that the model can reproduce the temperature evolution of the characteristic patterns observed in the LEED experiment. It is found that the (1×1) state following the c(2×8) ordered one is divided into domains of irregular polygons in each of which particles take a (2×2) arrangement. Moreover, the underlying mechanism of the characteristic domain structure of particle arrangements is elucidated. On the other side, for the Si(111) case the model modified in the way that the Takayanagi mechanism stabilizing the (7×7) structure of the Si(111) surface is incorporated is proposed. It is shown that the first order transition from the (7×7) state into the (1×1) one takes place. It is also shown that the model can reproduce diffuse spots around the $(\sqrt{3} \times \sqrt{3})$ Bragg points just above the transition. Furthermore, the disappearance of the stacking fault in the (1×1) phase is concluded from the calculation. A unified understanding of the reconstruction of Si(111) and Ge(111) is presented on the basis of the calculations.

Table of Contents

CHAPTER I

Introduction

§1.1 General Introduction to the (111) Surfaces of Si and Ge and the Lattice Gas Model

The (111) surface of Ge undergoes a phase transition at about 300°C from the c(2×8) state into the (1×1) one where diffuse spots around the (2×2) superlattice Bragg points are observed in the reflection high-energy electron diffraction (RHEED) and low-energy electron diffraction (LEED) experiments (Ichikawa and Ino, 1980; Phaneuf and Webb, 1985). For the Si(111) the transition from the (7×7) state to the (1×1) occurs at about 860°C above which $(\sqrt{3} \times \sqrt{3})$ diffuse spots are observed (Ino, 1977; Iwasaki *et al.*, 1987). Thus the ordered structures and the short-range orders in the high-temperature (1×1) phases of the surfaces apparently look quite different. Nevertheless, it is natural to consider that the underlying mechanisms of the phenomena should be similar to each other, since Si and Ge atoms of constituents of the two surfaces are similar to each other. In this thesis we give a unified understanding of the reconstruction aspects of the surfaces through the Monte Carlo calculations at finite temperatures of lattice gas models presented in the following chapters. The

present investigation is the one that gives the first unified theory of the underlying mechanism of the characteristic short-range order observed in the (1×1) phases of Si(111) and Ge(111).

The condition that each particle of the lattice gas model on a triangular net cannot come to nearest neighbour sites of other particles is satisfied by regarding the particles as 'hard hexagons.' In this sense the lattice gas model on a triangular lattice whose particles never come to the nearest neighbour sites of each other is called the hard hexagon model. It was shown by Baxter (1980) that the model without second and more distant neighbour interactions is exactly solvable.

Kanamori (1985) previously pointed out that the $(\sqrt{3}\times\sqrt{3})$ short-range order observed in the (1×1) phase of the Si(111) surface might be yielded by the random distribution of adatoms that avoid coming to nearest neighbour sites of each other on a triangular net consisting of favourable sites of adatoms on the surface. This was confirmed by a Monte Carlo simulation in collaboration with Okamoto (Kanamori, 1985) and by a calculation with the exact solution for the hard hexagon model (Fujimoto, *unpublished*). Thus a system of hard hexagons whose concentration is 1/4 produces $(\sqrt{3}\times\sqrt{3})$ diffuse spots in the momentum-space correlation function at sufficiently high temperatures where the second and more distant neighbour interactions are not important. The system takes the c(2×8) structure as the ground state for appropriate sets of interaction parameters (Kanamori, 1984). We note that the adatom concentrations for the c(2×8) and (7×7) arrangements are equal to and slightly less than 1/4, respectively. Therefore we

might regard this model as a unified one of the (1×1) states of Si(111) and Ge(111) and also the ordered state of Ge(111), interpreting the difference between the (1×1) states of Si(111) and Ge(111) as that between the transition temperatures of the surfaces. In order to discuss the ordered state of Si(111) it is necessary to extend the model in such a way that the (7×7) state is stabilized as a ground state, since the (7×7) arrangement of particles cannot be of the lowest energy in the simple lattice gas model.

§1.2 Organization of the Present Thesis

In the next chapter, Chap. II, an experimental overview and a brief review of the theoretical approach to the ordering problem of the (111) surfaces of Si and Ge are presented. Monte Carlo method for a system of classical particles is also summarized. Chapter III deals with the reconstruction of Ge(111) with a simple lattice gas model; the model and the Monte Carlo calculation are presented. We discuss there the (1×1) phase of the model at high temperatures on the basis of the simulation calculation, focusing our attention on the diffuse scattering patterns which reflect the short-range order. The adatom arrangement which produces the characteristic diffuse scattering pattern observed in the LEED and RHEED experiments and its underlying mechanism are also discussed. In Chap. IV an extended lattice gas model which can describe the reconstruction of the Si(111) surface both below and above the transition is constructed, and the Monte Carlo calculation of the model is carried out. Moreover, the disappearance of the stacking fault in the (1×1) phase of the surface is discussed on

the basis of the calculation. The final chapter, Chap. V, is devoted to a summary of the results obtained in Chaps. III and IV and some supplementary discussions. The interrelation between the reconstructions of the Si(111) and Ge(111) surfaces is discussed there.

CHAPTER II

Historical Overview

The present chapter presents an overview of previous investigations on the (111) surfaces of Si and Ge from experimental and also theoretical points of view. In §2.1 we give a brief review of the experimental feature of the surfaces with an attention focused upon the temperature dependence of the surfaces, i.e., the phase transitions and the ordered and disordered reconstruction structures. In §2.2 some important results of the theoretical approach to the ordering problem of the surfaces with the triangular lattice gas model are presented. Finally in §2.3 Monte Carlo method for a system of classical particles after Metropolis *et al.* used in the present investigation is summarized.

§2.1 Experimental Overview of the (111) Surfaces of Si and Ge

Each surface of solids takes a structure of atomic arrangement specific to the surface which is different from the structure in the bulk state. This is because atoms at the surface make a reconstruction to recover the stability which is broken by the abrupt termination of the periodic atomic arrangement seen in the bulk state. The (111) surfaces of Si and Ge have been known for about

thirty years as ones which show distinct and interesting reconstructions, and many investigations about them have been made by various methods from different points of view.

It was first found by Schlier and Farnsworth (1959) that the Si(111) surface takes a structure with the (7×7) periodicity at low temperatures. Since then many investigations have been made and various structure models of the surface have been proposed. It has been clarified that the structure corresponds to the (7×7) arrangement of adatoms on the surface (Binnig *et al.*, 1983). Also it has already been settled that the structure corresponds microscopically to the dimer adatom and stacking-fault (DAS) model (Takayanagi *et al.*, 1985) which is also called the Takayanagi model.

Figure 2.1 presents a top-view sketch of the DAS structure corresponding to the (7×7) state of the Si(111) surface; in the figure the location of atoms in up to the fourth underlayer is indicated schematically. Open circles in the figure denote atoms in the surface layer, i.e., the first underlayer and the second underlayer. It is distinct characteristics of the Takayanagi structure that both normally-stacking regions and stacking-faulted ones in the first underlayer exist which correspond to the upper and lower triangles, respectively, in the unit cell shown in the figure, and that dimers of Si atoms are formed in the second underlayer along walls each of which separates a stacking-faulted region from a nearby normal region. In this sense the first and second underlayers are usually referred to as the stacking-fault layer and the dimer layer, respectively. Though the surface energy is raised by generating stacking-faulted regions, the dimer formation lowers the surface

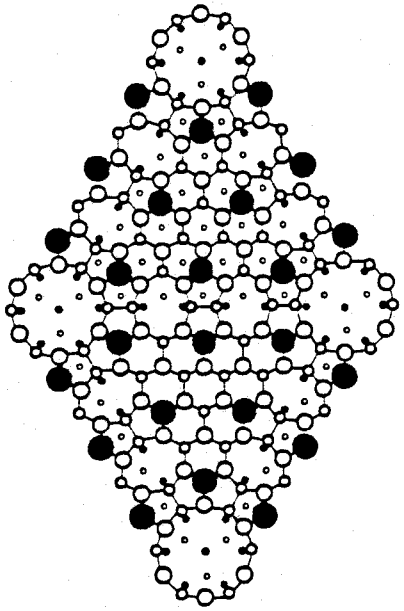

Figure 2.1
Top view of the (7×7) structure in the DAS model. Filled circles are adatoms. Open circles denote atoms in the first and second underlayers. Dots and small open circles show atoms in the bulk unreconstructed double layer corresponding to the third and fourth underlayers. The upper and lower triangle regions in the unit cell correspond to the normal and stacking faulted ones, respectively. Bonds between atoms in up to second underlayer are shown by lines.

energy sufficiently to stabilize the (7×7) structure. We notice that both stacking-faulted regions and normal ones are necessary for the dimer formation. This is considered to be the mechanism to stabilize the reconstruction structure of the Si(111) surface. We will refer to this mechanism as the Takayanagi mechanism hereafter. To reduce the number of dangling bonds in the surface, additional Si atoms which are called adatoms are adsorped on the surface layer. The layer in which adatoms sit is called the adatom layer. In order to reduce dangling bonds atoms at wall vertices in the dimer layer are missing; therefore the portions of the surface

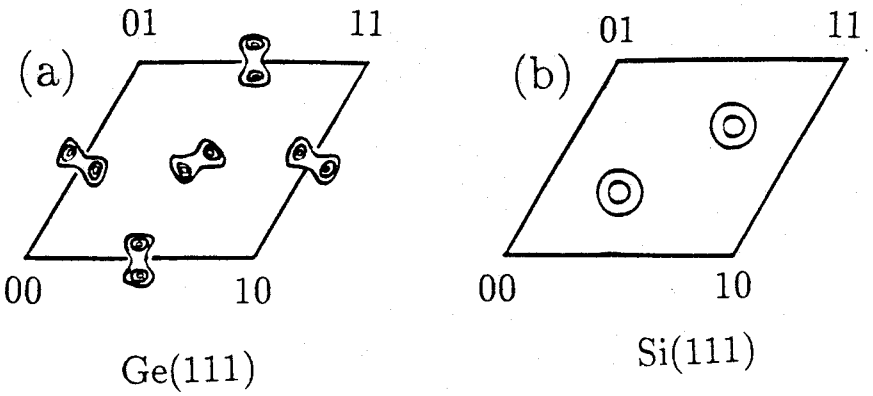

Figure 2.2
A sketch of the diffuse scattering of electron in the reciprocal space. (a) The data on the (1×1) state of Ge(111), and (b) the corresponding one of Si(111).

corresponding to wall vertices are called corner holes.

The Si(111) surface undergoes a first-order phase transition at about 860°C from the (7×7) state into the (1×1) one (Lander, 1964). The (1×1) state of Si(111) was first investigated by Ino (1977) with the RHEED experiment and afterwards by Iwasaki *et al.* (1987) with the LEED experiment. They found that diffuse spots around the $(\sqrt{3}\times\sqrt{3})$ superlattice Bragg points are observed in the (1×1) state; a sketch of the diffuse scattering pattern is presented in Fig. 2.2b.

On the other side, since it was found that the Ge(111) surface takes a structure which possesses the periodicity of eight times of a unit lattice spacing of the (111) surface (Palmberg and Peria, 1967; Palmberg, 1968; Henzler, 1969) at low temperatures, many investigations on the microscopic structure of the surface have been made. Chadi and Chiang (1981) and Yang and Jona (1984) discussed theoretically that the structure corresponds to a superposition of the three c(2×8) structures on a triangular net whose adatom arrangement is shown in Fig. 2.3. They stressed

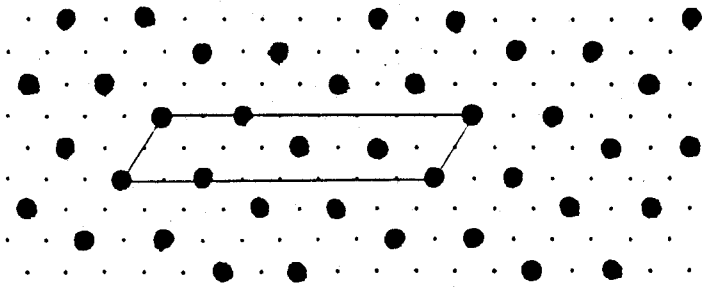

Figure 2.3
The c(2×8) arrangement of adatoms on the Ge(111) surface. A unit cell is shown by a parallelogram.

that the structure is not the primitive (2×8) one but the centred (2×8) one. Then the structure was investigated experimentally in detail (Phaneuf and Webb, 1985), and this was confirmed. The atomic-scale structure of the surface has recently been clarified by the scanning tunneling microscopy (STM) experiments (Becker *et al.*, 1986; Becker *et al.*, 1989); the structure corresponds to the c(2×8) arrangement of adatoms on a surface layer without stacking faults.

It is known for the Ge(111) surface that a phase transition from the c(2×8) state to the (1×1) one which is of the first order takes place at about 300°C (Palmberg, 1968) above which diffuse spots around the (2×2) superlattice Bragg points are observed (Ichikawa and Ino, 1980; Phaneuf and Webb, 1985). A sketch of diffuse scattering pattern observed above the transition temperature is presented in Fig. 2.2a. Aarts *et al.* (1988) performed photoemission measurements of the Ge $3d$ core level on the surface to find that no significant changes occur in the binding-energy spectra both below and above the c(2×8)-to-(1×1) transi-

tion. Thereby they concluded that the phase transition is of the order-disorder type, and that the (1×1) state corresponds to a random distribution of adatoms at the energetically favourable sites on the (1×1) substrate. Phaneuf and Webb (1985) investigated in detail the temperature evolution of the diffuse scattering patterns in the (1×1) phase by a LEED experiment. The diffuse peaks give us some information about the short-range order of adatoms on the surface. Immediately above the transition relatively weak diffuse spots at the (2×2) superlattice Bragg points and additional ones with strong intensity closer to the (2×2) superlattice Bragg points than the eighth order spots observed in the ordered state appear. The additional spots split into two in the direction from the (2×2) superlattice Bragg points towards the $(\sqrt{3} \times \sqrt{3})$ ones, as is shown in Fig. 2.2a. With increasing temperature the weak (2×2) peaks disappear, while the additional strong ones move away towards $(\sqrt{3} \times \sqrt{3})$ superlattice Bragg points with decreasing the peak height and increasing the peak width. The feature has been observed in RHEED experiments as well, though the data about the peak width seems not to agree with that of the LEED experiment. In the RHEED experiment by Ichikawa and Ino (1980) distinct split peaks are observed. While in the LEED experiment by Phaneuf and Webb they are more diffuse and the splitting of the peaks are not so distinct.

§2.2 Lattice Gas Approach to the Ordering Problem of Si(111) and Ge(111)

Kaburagi and Kanamori (1974; 1978) developed a lattice gas model on a triangular net with extended but finite range interactions by the use of the method of geometrical inequalities (Kanamori, 1966; Kaburagi and Kanamori, 1975) which determines the states of the lowest energy of a system of Ising spins or lattice gases in a rigorous way; the lattice gas model is referred to as 'a simple lattice gas model' in the present thesis in order to distinguish it from another one extended for the purpose of discussing the reconstruction of the Si(111) surface. The result is applicable generally to the ordering problem on surfaces and of magnetic systems with competing interactions, regarding the particles as equivalent local units of reconstruction on the surfaces and as Ising spins in the magnetic systems, respectively. Afterwards the lattice gas model was applied to the ordering problem of the (111) surfaces of Si, Ge, and Sn overlaid Ge; it was shown that the c(2×8), (7×7), and (5×5) ordered states can be regarded as the lowest energy particle arrangements of lattice gases (Kanamori, 1984; 1985). A different but more transparent point of view where the ordered particle arrangements were regarded as patterns consisting of discommensuration walls in the (2×2) arrangement of particles was proposed (Kanamori and Okamoto, 1985; Kanamori, 1986). In the investigation Kanamori had first clarified the interrelation between the ordered states of the surfaces. In addition he had shown that the (7×7) arrangement of particles cannot be

of the lowest energy in the lattice gas model. We summarize the discussion briefly below.

Figure 2.4 shows the c(2×8) and (7×7) arrangements of particles which correspond to reconstruction units of the surfaces, i.e., adatoms in the present cases. Although the arrangements apparently look quite different, we can give a following transparent picture to them. We can regard the particle arrangements as patterns of discommensuration walls running in the (2×2) arrangement where particles occupy mutually third neighbour lattice sites; the c(2×8) particle arrangement corresponds to the pattern of walls running parallel in one direction at the same interval of four lattice spacings, while the (7×7) one to the network of walls which run in three directions at intervals of seven lattice spacings. A discommensuration wall separates two domains in each of which particles take one of four (2×2) arrangements corresponding to the four sublattices of the original triangular net and particles close to the wall are situated at second neighbour sites across the wall. The discommensuration walls corresponding to the c(2×8) and (7×7) arrangements of particles are shown by lines in the figure. This picture clarifies the interrelation between the c(2×8) and (7×7) particle arrangements.

The lowest energy state of the lattice gas model can be analyzed by considering which of patterns consisting of discommensuration walls is of the lowest energy. Figure 2.5 shows the patterns corresponding to the c(2×8) state and the (7×7) one. The energy of the system of discommensuration walls is constructed by the wall energy which is required for producing a wall in the (2×2)

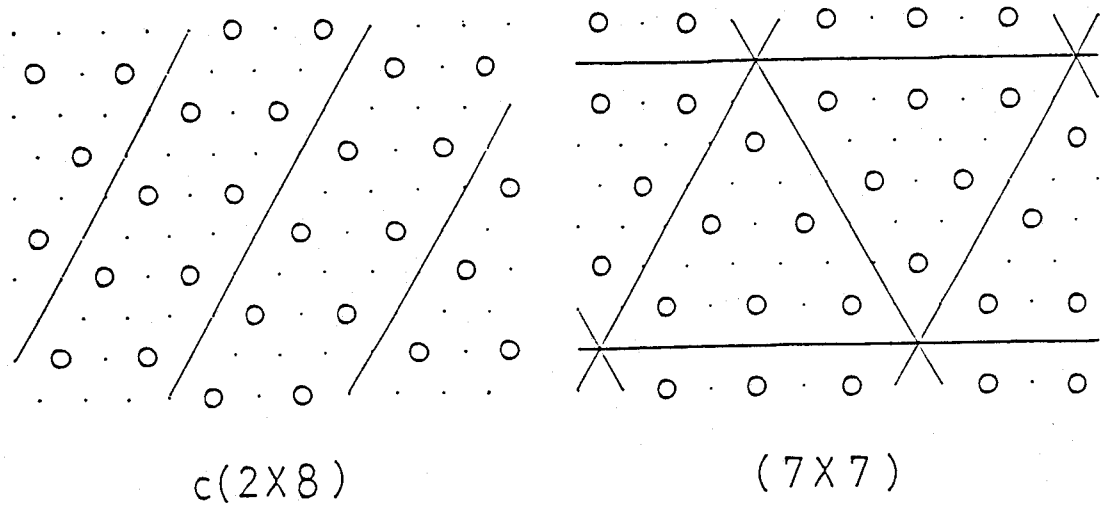

Figure 2.4
The particle arrangement on a triangular net in the c(2×8) state and the (7×7) one. Discommensuration walls are shown by lines.

state, the vertex energy which corresponds to the energy of such a wall vertex as is seen in the (7×7) state where three walls running in the three directions meet, and the interaction energies between walls and between vertices. On the basis of the energy analysis of the wall system Kanamori (1985) pointed out that the (7×7) arrangement of particles of the lattice gas model cannot be of the lowest energy except for the case that the (7×7) state is degenerate in energy with the (5×5) one and also c(2×8) one within the assumption that the energy of the system is presented by a sum of wall energies, vertex energies, and interaction energies between adjacent walls. We assume that we have no interaction between walls at interval of more than two lattice spacings in the original triangular lattice; we notice that discommensuration walls in the c(2×8) state do not interact with each other. Thus the energy of

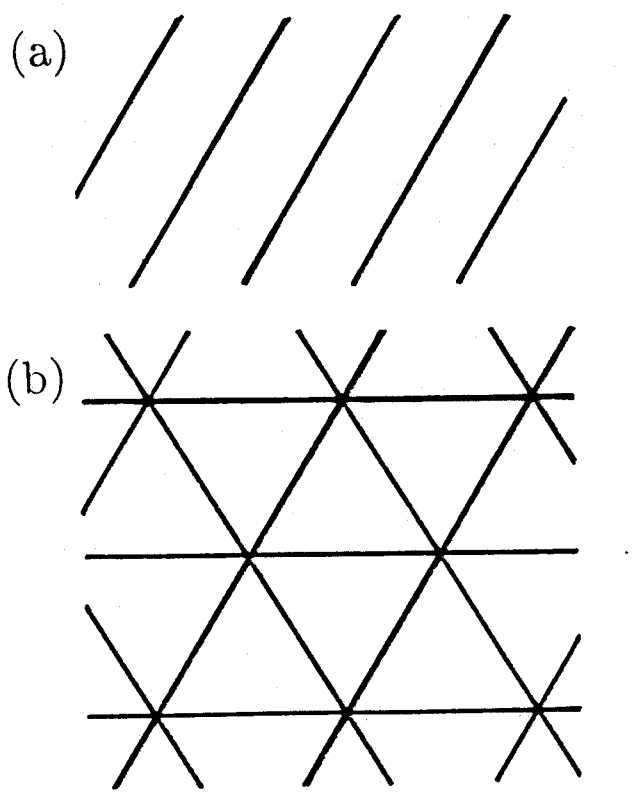

Figure 2.5
Configurations of systems of discommensuration walls. (a) The c(2×8) state and (b) the (7×7) one.

the c(2×8) state $E_{2\times 8}$ is expressed by

$$E_{2\times 8} = E_{2\times 2} + \frac{1}{4}Nw, \tag{2.1}$$

where $E_{2\times 2}$ denotes the energy of the (2×2) state, w the wall energy which is assumed to be negative, and N the number of lattice sites; the energy of the (2×2) state $E_{2\times 2}$ is presented, for example, in the case with up to the sixth neighbour pair interaction by

$$E_{2\times 2} = \frac{3}{4}NV_3 + \frac{3}{4}NV_6 + \frac{1}{4}N\mu, \tag{2.2}$$

where V_3, V_6 and μ denote the third and sixth neighbour interaction energies and the chemical potential, respectively. On the

other hand, the energy of the $(n \times n)$ state $E_{n\times n}$ with n=3, 5, 7, ... is given by

$$E_{n\times n} = E_{2\times 2} + \frac{3Nw}{n} + \frac{N(4v-\mu)}{4n^2}, \tag{2.3}$$

where v denotes the vertex energy. Thus we obtain

$$E_{n\times n} - E_{2\times 8} = \frac{N}{4n^2}[(12n - n^2)w + 4v - \mu]. \tag{2.4}$$

This expression shows us that the energy of the (5×5) state is lower than that of the (7×7) one if we assume $w < 0$ and $E_{7\times 7} < E_{2\times 8}$; the (7×7) state is of the lowest energy only in the case of $E_{7\times 7}$=$E_{5\times 5}$ where the c(2×8) state should also possess the same energy. From the result we conclude that the (7×7) state of the Si(111) surface should have some additional mechanism to stabilize the structure; this gives a theoretical support to the Takayanagi mechanism by which the (7×7) adatom arrangement of the Si(111) surface seems to be stabilized.

§2.3 Monte Carlo Method for a System of Classical Particles

Monte Carlo method is a technique to evaluate the summation of values of a physical observable over a given configuration space, sampling a relatively small number of configurations from the configuration space with a sequence of some random numbers; an 'observable' is meant as a function of the configuration. Since Metropolis *et al.* (1953) developed the fast method of calculations, it has been widely used for statistical-mechanical calculations.

So far as a classical system in a thermal equilibrium state is concerned, we can say that the Monte Carlo method is that for

calculating an ensemble average

$$\langle A \rangle = \sum_{c \in \Omega} p(c) A(c) \tag{2.5}$$

of a physical observable A in the following way:

1) We construct $\Omega^{\text{samp.}} = \{c_1, c_2, ..., c_M\}$, taking M samples from Ω according to a given probability $p^{\text{samp.}}(c)$,

2) calculate the value of

$$A(\Omega^{\text{samp.}}) = \frac{\sum_{c \in \Omega^{\text{samp.}}} \frac{p(c)}{p^{\text{samp.}}(c)} A(c)}{\sum_{c \in \Omega^{\text{samp.}}} \frac{p(c)}{p^{\text{samp.}}(c)}}, \tag{2.6}$$

3) and regard the above-calculated value of $A(\Omega^{\text{samp.}})$ as that of $\langle A \rangle$,

$$\langle A \rangle \approx A(\Omega^{\text{samp.}}), \tag{2.7}$$

where Ω is the configuration space, or more generally the phase space, of the system under consideration and $p(c)$ the probability that a configuration c of the system will be realized. According to this method we can evaluate any thermodynamic quantities represented by ensemble averages of some observables exactly within the statistical accuracy of the calculation; the accuracy is enabled to be sufficiently excellent if we use an appropriate technique for the problem and $\Omega^{\text{samp.}}$ of some extent. This is one of the advantages of this calculation method.

When we use the canonical ensemble

$$p(c) = \frac{\mathrm{e}^{-E(c)/k_{\mathrm{B}}T}}{\sum_{c \in \Omega} \mathrm{e}^{-E(c)/k_{\mathrm{B}}T}} \tag{2.8}$$

and adopt $p^{\text{samp.}}(c) = p(c)$, eq. 2.6 is reduced to

$$A(\Omega^{\text{samp.}}) = \frac{\sum_{c \in \Omega^{\text{samp.}}} A(c)}{M} \tag{2.9}$$

and

$$M = \sum_{c \in \Omega^{\text{samp.}}} 1, \tag{2.10}$$

where $E(c)$ denotes the energy of the system with a configuration c, T is the temperature of the system, and k_{B} is the Boltzmann constant. We have taken above $p^{\text{samp.}}(c)$ to be equal to $p(c)$. This enables us to make a calculation, utilizing each sample from Ω effectively. Each term in the summation over $\Omega^{\text{samp.}}$ gets to take a value of the same order of magnitude as well; this reduces a computational effort. This selection of $p^{\text{samp.}}(c)$ is called 'importance sampling,' because then the $\Omega^{\text{samp.}}$ is constructed by such configurations that importantly contribute to the ensemble average of the energy.

Now we discuss the way of constructing $\Omega^{\text{samp.}}$ with above-assumed $p(c)$ and $p^{\text{samp.}}(c)$. For the purpose of constructing $\Omega^{\text{samp.}}$ we use a Markov process which is such a stochastic process that the configuration c_i is determined by an appropriate transition probability that is a function of c_i and c_{i-1}, where the index i denotes the discrete time variable. We note that we can easily generate a Markov chain on a computer system, using a uniform sequence of random numbers which is produced, for example, with the method by Tausworthe (1965) and Lewis and Payne (1973) (Kirkpatrick and Stoll, 1981).

We consider such a Markov process that the transition probability from a configuration c to c' is given by

$$P_{cc'} \min[1, \mathrm{e}^{-(E(c')-E(c))/k_{\text{B}}T}], \tag{2.11}$$

where $P_{cc'}$ is usually called *a priori* probability that is used for the

purpose of limiting configurations into which it is *a priori* allowed to make a transition from a given configuration in a trial, and $\min[x, y]$ is such a function as

$$\min[x, y] = \begin{cases} x, & \text{if } x \leq y; \\ y, & \text{if } x > y. \end{cases} \tag{2.12}$$

We call hereafter such configurations c and c' as $P_{cc'} \neq 0$ 'neighbouring configurations to each other.' We let $P_n(c)$ denote the probability that the configuration of the system reached after n times of such transitions from a given initial configuration is c. If $E(c) < E(c')$ for two neighbouring configurations c and c', the flow of the probability $P_n(c)$ from the configuration c into c' is

$$P_n(c)P_{cc'}\mathrm{e}^{-(E(c')-E(c))/k_{\mathrm{B}}T} - P_n(c')P_{c'c}. \tag{2.13}$$

Especially in the case of $P_{cc'}$=$P_{c'c}$, this is written as

$$P_{cc'}P_n(c)\{\frac{\mathrm{e}^{-E(c')/k_{\mathrm{B}}T}}{\mathrm{e}^{-E(c)/k_{\mathrm{B}}T}} - \frac{P_n(c')}{P_n(c)}\}. \tag{2.14}$$

As can be seen from the expression, this flow of the probability forces the probability $P_n(c)$ to approach a function of c with increasing n. Thus we obtain for two neighbouring configurations c and c'

$$\frac{P_n(c')}{P_n(c)} = \frac{\mathrm{e}^{-E(c')/k_{\mathrm{B}}T}}{\mathrm{e}^{-E(c)/k_{\mathrm{B}}T}} \tag{2.15}$$

for large n. If the transition probability eq. 2.11 is, in addition, ergodic, we thus obtain for any two configurations c and c' in the configuration space Ω

$$\frac{P_n(c')}{P_n(c)} = \frac{\mathrm{e}^{-E(c')/k_{\mathrm{B}}T}}{\mathrm{e}^{-E(c)/k_{\mathrm{B}}T}} \tag{2.16}$$

for sufficiently large values of n; we mean that the transition probability is ergodic when the following ergodicity condition holds: n which is not very large exists where $P_n(c) \neq 0$ is satisfied both for $^{\forall}c \in \Omega$ and any initial configurations.

In the result, when the ergodicity condition is satisfied in the Markov process used in a calculation, the following expression holds for sufficiently large n_0:

$$P_n(c) \propto \mathrm{e}^{-E(c)/k_{\mathrm{B}}T}, \qquad \text{for } ^{\forall}n > n_0 \gg 1. \tag{2.17}$$

Thus we can construct $\Omega^{\mathrm{samp.}} = \{c_{n_1}, c_{n_2}, ..., c_{n_M}\}$, sampling M configurations $c_{n_1}, c_{n_2}, ..., c_{n_M}$ from the configuration space of the system Ω via the Markov process where n_1, n_2, ..., and n_M are larger than n_0 in eq. 2.17.

Finally we note that the above-mentioned calculation method for classical systems is easily extended to that of quantum systems formally. 'A quantum system' is meant for such one as either some interesting physical quantities cannot be diagonalized simultaneously with the hamiltonian of the system but the eigenvalues and eigenstates of the hamiltonian are known or both eigenvalues and eigenstates of the hamiltonian cannot be found easily at a glance. In the former case the above-mentioned method for a classical system works, if only we take the representation to diagonalize the hamiltonian, replace such products of physical quantities as $A(c)B(c)$ in the above discussion with $A(c_1, c_2)B(c_2, c_1)$, and extend the configuration space to $\Omega \times \Omega$, where $A(c_1, c_2)$ denotes a matrix element $\langle c_1|A|c_2\rangle$ and c_1 and c_2 the labels which distinguish between the eigenstates of the hamil-

tonian. In this case we regard $c = (c_1, c_2) \in \Omega \times \Omega$ as a configuration of the system. While in the latter case in order to utilize the method described above it is necessary to decompose the hamiltonian H into a summation of $\delta H = H/\nu$ where $\nu \gg 1$ is so-called the Trotter number and to extend more the configuration space to $\Omega \times \Omega \times ... \times \Omega = \{c_1 | c_1 \in \Omega\} \times \{c_2 | c_2 \in \Omega\} \times ... \times \{c_{\nu+n} | c_{\nu+n} \in \Omega\}$ in calculating an ensemble average $\langle A_1 A_2 ... A_n \rangle$, where c_1, c_2, and so on denote the labels to distinguish between the states which form a complete set convenient for the calculation. Thus we can use the method developed for classical systems to calculate some ensemble averages of quantum-mechanical quantities. However, it is more difficult in general to carry out calculations of such systems; to sophisticate the method and much computational effort are necessary there.

CHAPTER III

Simple Lattice Gas Model: Ge(111) Case

In this chapter we investigate the reconstruction of the (111) surface of Ge, carrying out the Monte Carlo calculation of a lattice gas model which is referred to as the simple lattice gas model in the present thesis. In the first section, §3.1, the model is presented. We analyze the ground states of the model in §3.2, regarding particle arrangements as patterns made of discommensuration walls which run parallel in the (2×2) state. The ground-state phase diagram of the model is presented there. In this chapter we make an investigation on the reconstruction of the Ge(111) surface, carrying out Monte Carlo calculations of the simple lattice gas model. A detailed description of the computational method for the model is presented in §3.3. Sections 3.4 and 3.5 present the Monte Carlo calculation of the model. In §3.4 the phase transition from each of the ordered states into the disordered (1×1) state is investigated. Section 3.5 presents a detailed investigation of the (1×1) phase of the model. The temperature evolution of the reciprocal-space correlation function which corresponds within the kinematical approximation to the scattering pattern in electron-diffraction experiments is calculated, and it is demonstrated that the present

model is capable of reproducing the temperature dependence of the Ge(111) surface. On the basis of the calculation the adatom arrangement which causes the characteristic diffuse scattering observed in electron-diffraction experiments on the (1×1) phase of the surface is proposed, and its underlying mechanism is discussed from a statistical-mechanical view point; in the discussion the relation between the entropy of the model and the number of triplets of mutually second neighbouring particles is also clarified. The discussion in the present chapter has been presented partly in the previous publications (Sakamoto and Kanamori, 1989a, 1989b, 1991; Kanamori and Sakamoto, 1991).

§3.1 Model

It seems that the c(2×8) arrangement of adatoms with the stacking-faulted substratum where zigzag walls are necessary to run is energetically unfavourable; it is conjectured that the c(2×8) state of the Ge(111) surface probably corresponds to the simple adatom model where adatoms are located at the favourable sites on the surface layer without the stacking fault. Although it has recently been clarified by the STM (Becker *et al.*, 1986; Becker *et al.*, 1989), ion-beam scattering (Maree *et al.*, 1988), and X-ray diffraction (Feidenhans'l *et al.*, 1988) experiments that no stacking fault is present in the substratum layer of the surface, the present investigation through the lattice-gas Monte Carlo calculation had motivated the present author to confirm theoretically the conjecture that the reconstruction of Ge(111) is accompanied by no stacking-faulted substratum unlike the case of the (7×7) state

of Si(111). We try to discuss the reconstruction of the surface with a simple lattice gas model on a triangular net whose particles correspond to the adatoms, and to confirm the conjecture on the basis of the investigation. In this section the simple lattice gas model used in the present investigation is presented.

The energy of the model E is given by

$$E = V_1 p_1 + V_2 p_2 + V_3 p_3 + V_4 p_4 + V_5 p_5 + V_6 p_6, \qquad (3.1)$$

where p_k denotes the number of the k-th neighboring pairs of particles and V_k the interaction energy of the corresponding pairs. The definition of the k-th neighbour sites is shown in Fig. 3.1. In the figure a triplet of mutually second neighbouring particles whose number in the system is denoted by X_1 and a linear one of the second neighbours the interaction energy of which is denoted by U_2 are also shown. Figure 3.2 shows particle arrangements in the ordered structures. The interaction energies of the pairs are effective interactions between corresponding adatoms through the substratum layers. We assume that the essential part of the total energy of the surface is composed of the energies of the effective interactions. A Monte Carlo study demonstrating that the model can reproduce essential features of the temperature dependence of the Ge(111) surface would justify the assumption. We have assumed above that the interaction is extended up to the sixth neighbour sites; the repulsive sixth neighbour interaction is essential to the discussion of the reconstruction of the surface. The assumption is discussed in the next section in detail.

We assume that the available sites for particles of the model make a triangular net, since the adatom arrangement on the (111)

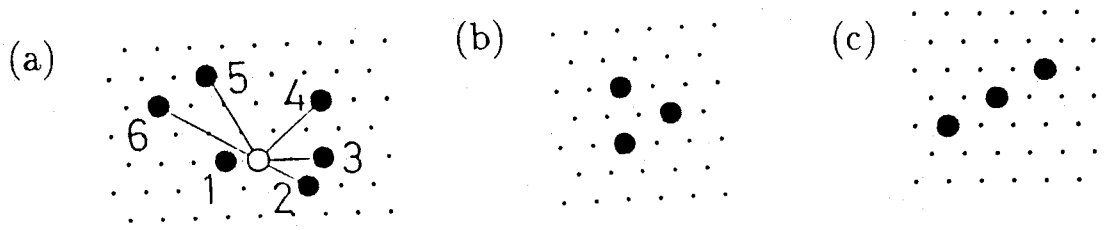

Figure 3.1
Definition of neighbours and triplets of particles. (a) Neighbours of a particle denoted by an open circle, (b) a triplet of mutually second neighbouring particles, and (c) a linear triplet of the second neighbours.

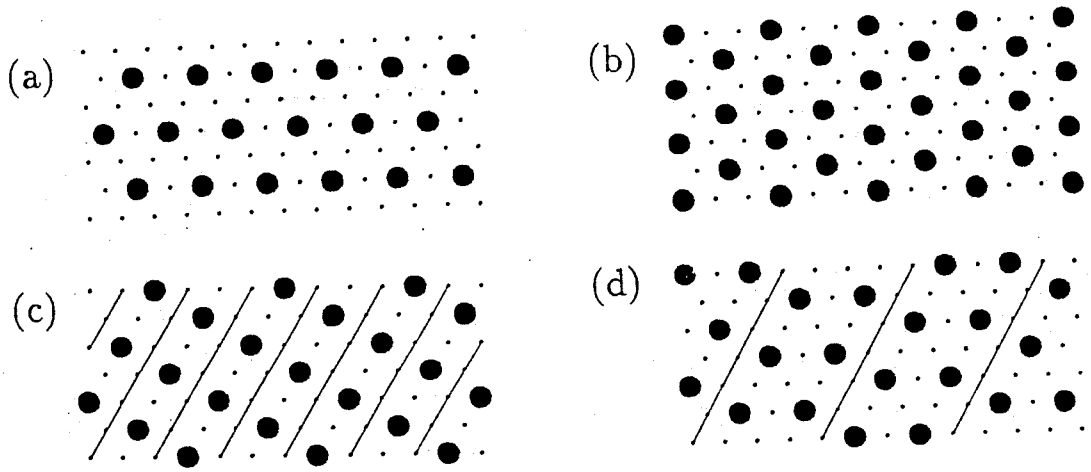

Figure 3.2
Particle arrangements in (a) the (2×2) state, (b) the $(\sqrt{3} \times \sqrt{3})$R30° state, (c) the c(2×4) state, and (d) the c(2×8) state. Circles and dots denote particles and unoccupied sites, respectively. Discommensuration walls are also denoted by lines.

surface of Ge can be described as a particle arrangement on a triangular lattice. In addition we also assume that the concentration of particles is 1/4 which corresponds to that of adatoms on the surface in the c(2×8) state. However, the concentration of adatoms on the surface may change with temperature. This will be discussed in Chap. V.

It is energetically unfavourable that adatoms come to the nearest neighbour positions where they have to share a dangling bond of a substratum atom. The situation corresponds to the sufficiently repulsive nearest neighbour interaction between particles of the lattice gas model. Thus we assume in the model $V_1=+\infty$. With this assumption the term of $V_1 p_1$ in the energy expression eq. 3.1 is eliminated, because we have no nearest neighbouring pairs of particles, $p_1=0$. The condition $V_1=+\infty$ or $p_1=0$ in the triangular lattice gas model is called the hard hexagon condition. The condition ensures the $(\sqrt{3} \times \sqrt{3})$ short-range order at sufficiently high temperatures. Since the $(\sqrt{3} \times \sqrt{3})$ short-range order is observed in electron-diffraction experiments on the (1×1) phase of Si(111), the present model might also describe the (1×1) state of the Si(111) surface. This is discussed in the next chapter, Chap. IV.

The present model corresponds to a specific case of the extended lattice gas model which will be discussed in the following chapter for the Si(111) surface, as will be discussed in Chap. V. For simplicity, however, we restrict ourselves to the simple lattice gas model in the present chapter.

§3.2 Ground States of the Model

In this section we consider the lowest-energy states of the hard-hexagon system with up to the sixth neighbour interaction whose concentration is 1/4.

In the case of $V_2 > 0$ and $V_k=0$ for $k \geq 3$, we can see straightforwardly that the (2×2) state where each particle is sit-

uated at one of the third neighbour sites of its neighbouring particles is the lowest-energy state. While for $V_2 < 0$ we obtain the $(\sqrt{3} \times \sqrt{3})$ state as the lowest-energy one. We assume $V_2 > 0$ hereafter, because the $(\sqrt{3} \times \sqrt{3})$ structure does not appear as the ordered states of the (111) surfaces of Si and Ge.

The lowest-energy states of the system with up to the sixth neighbour interaction can be regarded as such states that can be generated from the (2×2) state by introducing discommensuration walls, if V_3 is not so large and $V_2 > 0$ is assumed; we regard the (2×2) state as the reference state. When V_3 is sufficiently large, no ordered structures with the concentration 1/4 can be of the lowest energy. We do not consider such a case in the following part of this section.

The energy of the system with $N{=}L \times L$ lattice sites in which ν discommensuration walls parallel to each other run can be expressed as

$$E = E_{2\times2} + \nu w L + \pi_1 v_1 L, \tag{3.2}$$

$$E_{2\times2} = \frac{3}{4}NV_3 + \frac{3}{4}NV_6, \tag{3.3}$$

$$w = \frac{1}{2}V_2 - V_3 + V_4 - 2V_6, \tag{3.4}$$

and

$$v_1 = V_6, \tag{3.5}$$

where $E_{2\times2}$ is the energy in the (2×2) reference state; w denotes the energy per unit lattice spacing necessary for producing a discommensuration wall; v_1 is the interaction energy per unit lattice spacing between walls which are situated at the nearest neighbour

positions of each other, or in other words that between walls which run parallel at the interval of two lattice spacings (an example of a nearest neighbouring pair of discommensuration walls is shown in Fig. 3.3); and π_1 denotes the number of the corresponding pairs of walls. We notice that the number of the walls can take the values $\nu = 0, 1, 2, ..., L/2$; ν=0, $L/2$, and $L/4$ correspond to the (2×2), c(2×4), and c(2×8) states, respectively.

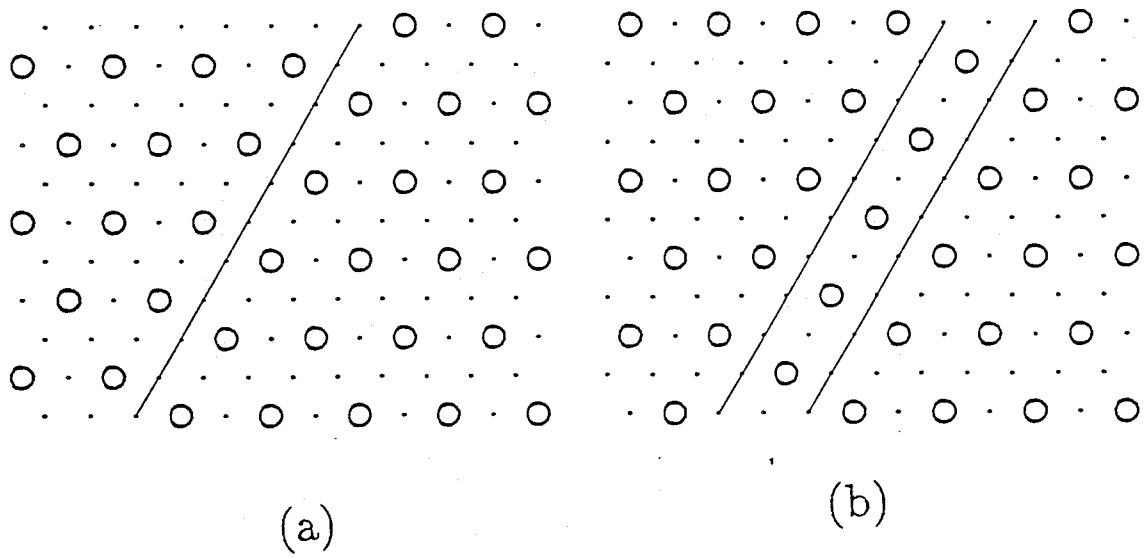

Figure 3.3
Discommensuration walls in the (2×2) state. (a) A discommensuration wall which separates two (2×2) domains, and (b) a pair of adjacent walls, i.e., parallel walls at the smallest interval.

We have included the interaction energy at the sixth neighbour sites into the energy expression eq. 3.1. This is essential to the discussion of the reconstruction of the Ge(111) surface. The c(2×8) structure which is the ordered state of the surface can be regarded as the one where the walls separating the (2×2) domains

run parallel at the regular intervals of four lattice spacings; if they run at the shortest intervals of two lattice spacings, the structure is the c(2×4). The repulsive sixth neighbour pairwise interaction and the repulsive three particle interaction of the particle arrangement shown by Fig. 3.1c whose energy is denoted by U_2 can give rise to a repulsive interaction of the walls at this shortest interval, while no such an interaction arises from other pairwise interactions up to the fifth neighbour. The sixth neighbour interaction changes the reagion in the interaction-parameter space where the (2×2) state is the ground state in the case with up to the third neighbour interaction into that of the c(2×8) one, while the three-particle interaction changes the reagion of the c(2×4) into the c(2×8). The three particle interaction cannot reproduce the feature in the (1×1) phase of the surface, as is mentioned in §§3.5.1. Thus the repulsive sixth-neighbour pair interaction is the simplest one which generates the repulsive interaction between adjacent walls. Therefore we adopt the repulsive sixth neighbour interaction as the representative which stabilizes the c(2×8) particle arrangement.

We consider first the case of $v_1 > 0$ (repulsive inter-wall interaction) or $V_6 > 0$. For $w > 0$ or $V_3 < -2V_6 + V_4 + (1/2)V_2$, since no interactions compete with each other, the lowest energy state of the model is simply the state with no discommensuration walls, namely, the (2×2) state. While in the case of $w < 0$ the competition between w and v_1 complicates the analysis of the lowest energy state of the model. In this case the lowest energy state is determined by it whether the value of $w + 2v_1$ is positive or neg-

ative. For $w + 2v_1 < 0$ or $V_3 > V_4 + (1/2)V_2$ the structure which has a maximum number ν=$L/2$ of discommensuration walls, i.e., the c(2×4) one is of the lowest energy under the condition X_1=0; we notice that this condition does not hold for sufficiently large values of V_3. While in the case of $w + 2v_1 > 0$ or $V_3 < V_4 + (1/2)V_2$ in addition to the negative wall energy condition $w < 0$, a nearest neighbour pair of walls raises the energy of the system by its repulsive interaction though each wall lowers the energy of the system. Therefore in this case the structure that possesses a maximum number of walls within the condition π_1=0, i.e., the c(2×8) structure is of the lowest energy.

Next we consider the case with the attractive wall-wall interaction $v_1 = V_6 < 0$. When the wall energy w is negative, the lowest-energy state is clearly the c(2×4) so far as the condition X_1=0 holds. In the positive wall-energy case the lowest energy state is determined by whether the value of $w + v_1$ is positive or negative. If $w + v_1$ is positive, i.e., $V_3 < -V_6 + V_4 + (1/2)V_2$, the (2×2) state is of lowest energy because of the increase of the energy by producing a wall. While for negative $w + v_1$ the c(2×4) state with a maximum number of walls is of the lowest energy, since to generate a wall decreases the energy of the system.

We present the ground-state phase diagram of the present lattice gas model in Fig. 3.4, where V_4=0 is assumed which is also assumed in the Monte Carlo calculations carried out in this chapter; the assumption is more discussed in §§3.3.6.

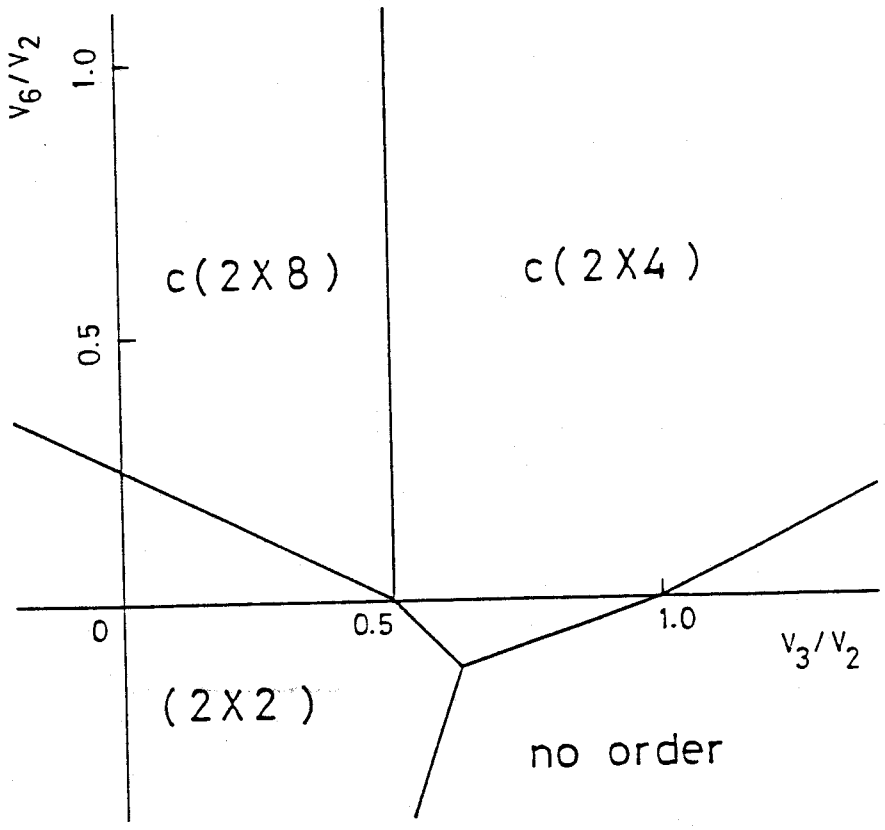

Figure 3.4
Ground-state phase diagram of the simple lattice gas model. V_4=0 is assumed.

§3.3 Detailed Description of the Calculation Scheme

We carry out Monte Carlo calculations of the lattice gas model at finite temperatures with canonical ensembles. The formal description of the general method of the calculations is presented in §2.3. In the present section we describe the details of the calculation for the lattice gas system considered in this chapter.

§§*3.3.1 Finite System Size*

It is essential to the Monte Carlo calculation to sample some configurations from the configuration space of the system under

consideration. Since we cannot construct a configuration of a system with the infinite size on a computer system, we are forced to treat one with a finite system size.

In the calculation carried out for the simple lattice gas model in the present chapter, we adopt the lattice sizes of 24×24 and 48×48 sites. These system sizes are sufficient to discuss the problem of the Ge(111) surface, since the characteristic correlation length of the system is probably shorter than the linear sizes we adopt.

§§3.3.2 *Boundary Condition*

A finite system has a boundary. The effect contributed by the boundary is unfavourable, because we would like to investigate properties of a system extended infinitely. We can, however, eliminate the effect formally by using the periodic boundary condition and adopting a system size larger than the correlation length characteristic of the problem.

We note that the sixfold symmetry of the system which is violated in a system with a free boundary is recovered by the boundary condition; the boundary condition makes the configuration made from rotating a given configuration by $2\pi/6$ around a given lattice site an acceptable one with the same energy that the original one has.

§§3.3.3 *Particle Number*

As is discussed in the previous sections, we consider the system whose concentration of particles x is $1/4$. However, if we

adopt x=1/4 precisely, we face a difficulty in carrying out the calculations.

We imagine a hard hexagon system of x=1/4 which takes the configuration of either the (2×2), c(2×4), or c(2×8) arrangement. As far as we use the *a priori* probability defined in the following subsection, the transition from the configuration into any other ones cannot take place in any Monte Carlo trials and vice versa. If the configurations (2×2), c(2×4), and c(2×8) were not important, we could consider that the ergodicity condition in the calculation holds in practice. These states, however, play an important role in our discussion of the problem of Ge(111), because they are the ground states of the model.

This difficulty can be removed by reducing the number of particles slightly to the extent that this does not affect the ordered state. With this reasoning we assume in the calculations that the concentration is 143/576 which is slightly less than 1/4.

§§*3.3.4 Particle Number Fixing*

The calculations in the present chapter are carried out, fixing the total number of particles in the system at the values corresponding to the above-mentioned concentration x=143/576. In order to satisfy the condition we use such an *a priori* probability that $P_{cc'} \neq 0$ if a configuration c' is the one caused by moving a particle in the system with a configuration c to one of its nearest neighbour lattice sites, and that $P_{cc'} = 0$ for other cases. In other words, in a Monte Carlo trial we just either move a particle to its nearest neighbour site or do not change the configuration. We

note that we must take $P_{cc'} \neq 0$ for the configuration c' which does not satisfy the hard hexagon condition p_1=0 so as to satisfy the symmetry condition of the *a priori* probability $P_{cc'}=P_{c'c}$; the hard hexagon condition is then ensured by the other factor in the transition probability eq. 2.11 which vanishes.

§§3.3.5 Correlation Function Calculation

In order to discuss the diffuse scattering patterns observed in the LEED and RHEED experiments we calculate the correlation function of the lattice gas model in the momentum space

$$\begin{aligned} S(k) &= \frac{1}{N}\langle |\sum_r n(r)\mathrm{e}^{ik\cdot r}|^2\rangle \\ &= \sum_r G(r)\mathrm{e}^{ik\cdot r} \end{aligned} \tag{3.6}$$

and

$$G(r) = \frac{1}{N}\langle \sum_{r'} n(r')n(r'+r)\rangle, \tag{3.7}$$

where $n(r)$ is the occupation number at the lattice site r which takes the unity if the site is occupied by a particle and takes the nought if not. Since the function $G(r)$ is the ensemble average of an observable $\sum_{r'} n(r')n(r'+r)$, we can evaluate it through a Monte Carlo calculation.

In the calculation of the function $S(k)$ we take an average over three independent directions which correspond to rotating a configuration by 0, $2\pi/3$, and $4\pi/3$, respectively, around a lattice site in the real space to save the computational effort. Thereby we obtain the result averaged over the six independent directions corresponding to the full rotational symmetry of the lattice gas

model, since the average over other three directions corresponding to the inversion of the three configurations has already been incorporated in the summation in eq. 3.7. For the c(2×8) ordered state this corresponds to the superposition of the three ordered configurations; we will not, however, carry out the calculation of $S(k)$ for the ordered state.

§§3.3.6 *Additional Assumption to the Interaction Parameters*

As is mentioned in the previous section, we assume that the second neighbour interaction is repulsive, i.e., the interaction energy of a corresponding pair V_2 is positive, because of the fact that the $(\sqrt{3}\times\sqrt{3})$ structure does not appear as the ordered state of the (111) surface of Ge. We measure hereafter the energy and the temperature in a unit of the strength of the repulsive second neighbour interaction V_2.

In addition, we assume that the energy of a fourth neighbouring pair and a fifth neighbouring one of particles V_4 and V_5 take the value of nought. Since the fourth neighbour interaction V_4 just shifts the wall energy w and the fifth neighbour one V_5 affect no effect to the energy of the ground state, we can omit V_4 and V_5 so far as the ordered state of the model is concerned. Although these interactions affect details of the temperature dependence of the system, we believe that they do not change the essential feature of the temperature dependence.

As is mentioned in §3.1, we also assume that the hard hexagon condition holds, i.e., $V_1=+\infty$ or $p_1=0$. Thus the energy of

the model E given by eq. 3.1 is reduced to

$$E = V_2 p_2 + V_3 p_3 + V_6 p_6. \tag{3.8}$$

Then the ensemble average of the energy $\langle E \rangle$ is evaluated from

$$\langle E \rangle = V_2 \langle p_2 \rangle + V_3 \langle p_3 \rangle + V_6 \langle p_6 \rangle. \tag{3.9}$$

We notice that these assumptions force us to have just two adjustable parameters V_3/V_2 and V_6/V_2 in calculations.

§3.4 Phase Transitions

Figure 3.5 shows an example of the temperature evolution of the energy per particle $\langle E \rangle / Nx$, where N and x denote the number of lattice sites and the concentration of particles, respectively. There N=48×48 is assumed. We also assume there V_3/V_2=0.32 and V_6/V_2=0.1 where the ordered state is the c(2×8) one. Ensemble averages are taken over 50 000 Monte Carlo steps in the calculations; a Monte Carlo step corresponds to the completion of Monte Carlo trials for the whole particle of the system. Although the figure shows the energy versus temperature relation for the lattice size of 48×48, the result is independent of the system size. The figure clearly indicates that the first-order phase transition from the c(2×8) state into the (1×1) one takes place at the transition temperature; the first-order phase transition is meant as such one that the state of the system changes discontinuously at the transition point from the ordered state just below the transition into the disordered one just above it. It can be revealed through a histogram representation of energy distribution at a temperature around the transition whether the phase transition is of the

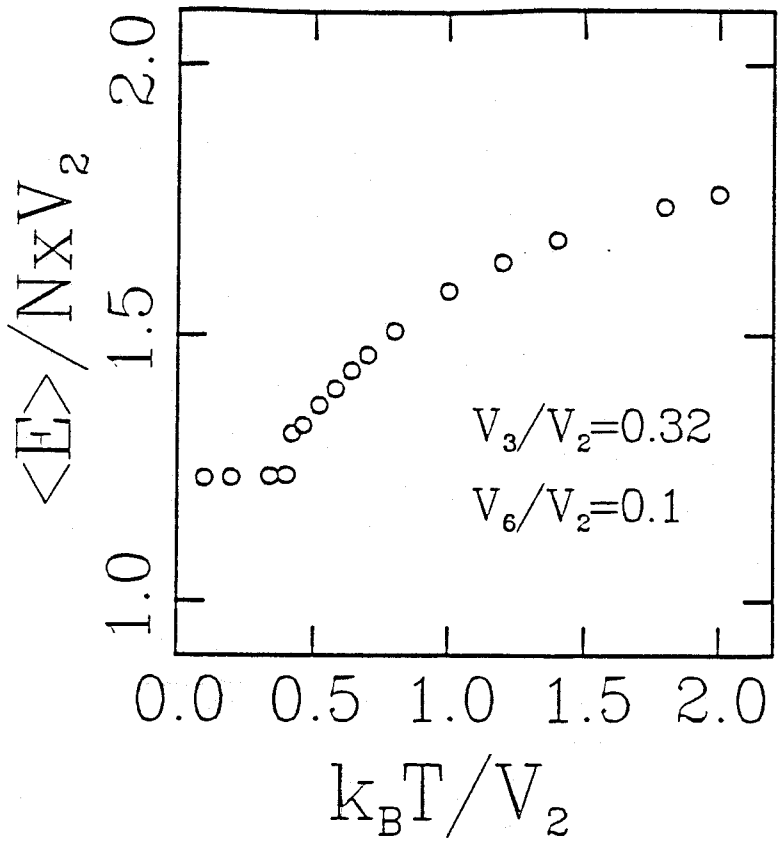

Figure 3.5
Temperature dependence of the energy in the case of V_3/V_2=0.32 and V_6/V_2=0.1, where N=48×48 and x=143/576 are assumed.

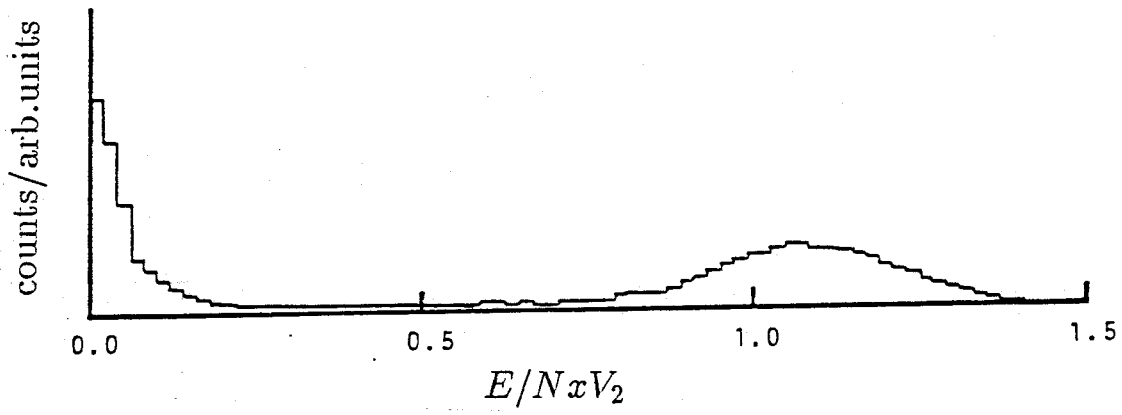

Figure 3.6
Histogram for energy at k_BT/V_2=1.75 in the case of V_3=V_6=0, N=24×24, and x=143/576.

first kind or the second one. Figure 3.6 shows an example of the

histogram for energy at a temperature around the transition; we assume there $V_3=V_6=0$ where the ordered state is the (2×2) one, $k_BT/V_2=1.75$, and $N=24\times24$. We have a double peak split clearly in the figure, which shows us that the phase transition is of the first order.

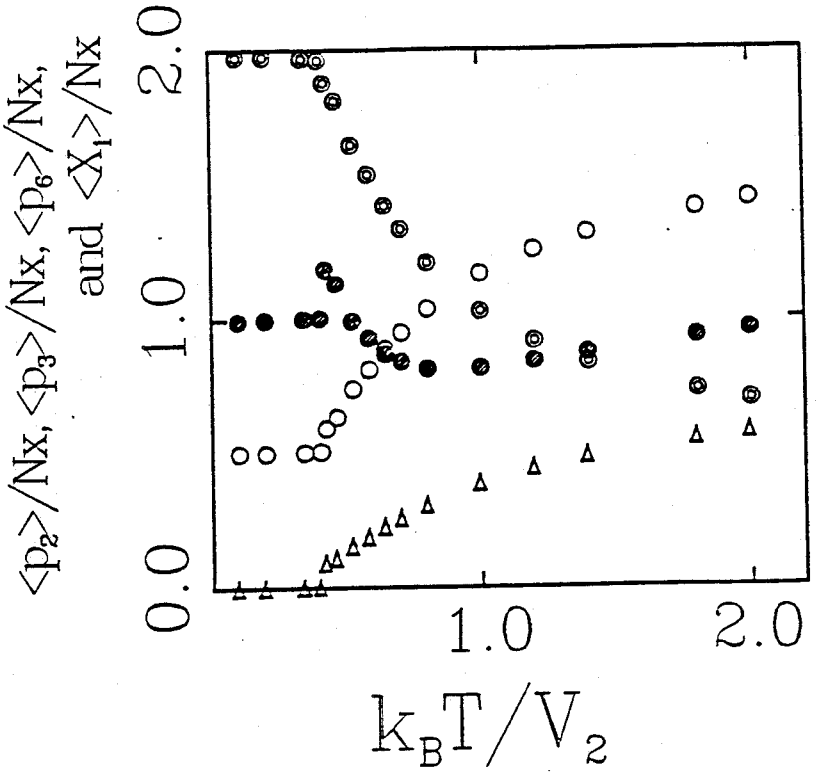

Figure 3.7
Temperature dependence of the numbers of pairs and triplets of particles in the case of $V_3/V_2=0.32$, $V_6/V_2=0.1$, $N=48\times48$, and $x=143/576$. Open, double, and hatched circles and triangles show those of second, third, and sixth neighbouring pairs and mutually second neighbouring triplets, respectively.

Figure 3.7 shows the temperature dependence of the numbers per particle of second, third, and sixth neighbouring pairs of particles $\langle p_2\rangle/Nx$, $\langle p_3\rangle/Nx$, and $\langle p_6\rangle/Nx$ and that of mutually second neighbouring triplets $\langle X_1\rangle/Nx$. This shows us that in a range of temperature above the transition the system still stay in

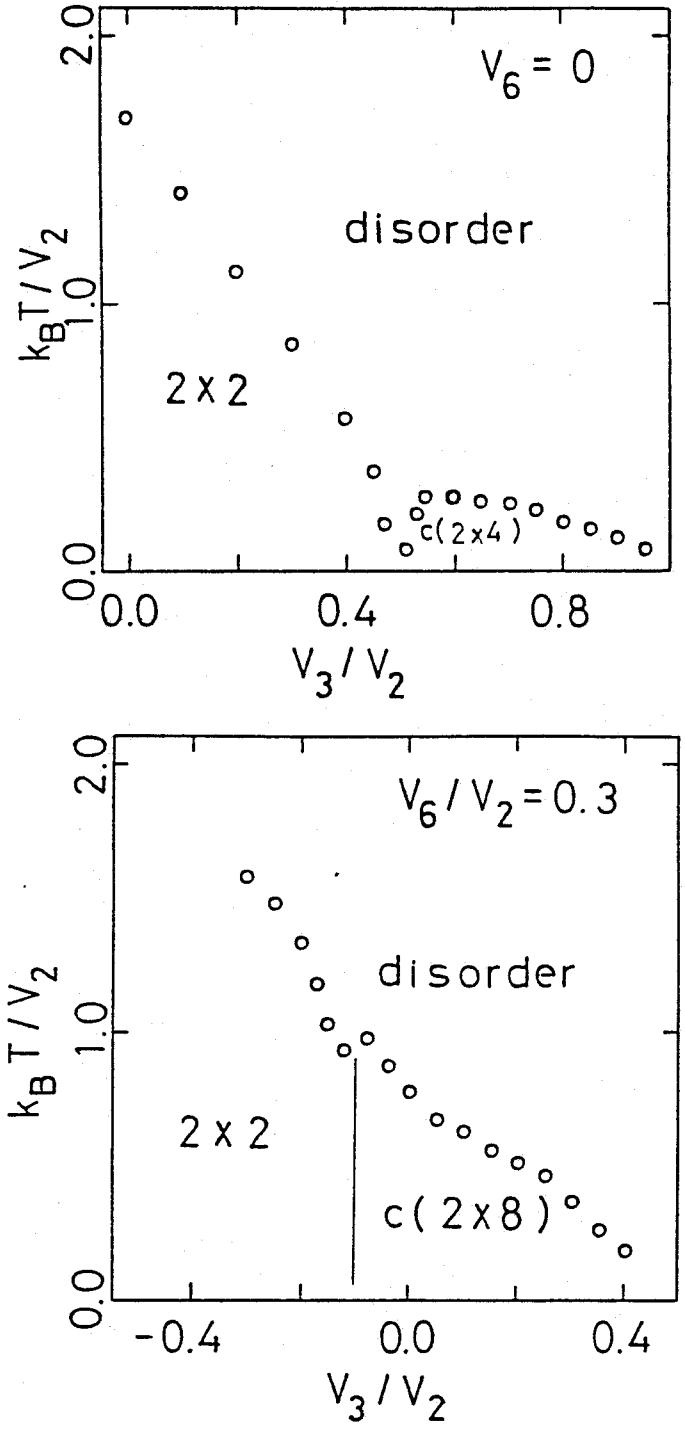

Figure 3.8
Phase diagrams in the T vs. V_3 plane for V_6/V_2=0 and 0.3.

a state far from that which corresponds to the completely random distribution of particles. This corresponds to the characteristic short-range order observed in the LEED and RHEED experiments on the (1×1) phase of the Ge(111) surface, the details of which will be discussed in the following section.

We give examples of the calculated phase diagram in a T-V_3 plane in Fig. 3.8. The phase transitions from each ordered state to the disordered (1×1) state are of the first order in accordance with the group theoretical argument (Domany *et al.*, 1977, 1978). Each transition temperature has been determined on the basis of calculations carried out with increasing temperature. In the present calculations the transition from the disordered state to the ordered c(2×8) one has not occurred. We note, however, that this does not mean that the transition from the (1×1) state to the c(2×8) one cannot take place in the present model; this is caused just by both the complicated ordered structure and the Monte Carlo scheme in which a configuration is updated locally. In fact a system of a smaller size with 8×8 lattice sites transforms reversibly both from the c(2×8) state to the (1×1) and from the (1×1) to the c(2×8). In the case where the ordered state is the (2×2) one, the system even with 48×48 lattice sites transforms reversibly.

§3.5 High-Temperature (1×1) Phase

We have mentioned in §2.1 that characteristic diffraction patterns which show diffuse spots around the (2×2) superlattice Bragg points are observed in the RHEED and LEED experiments on the high-temperature (1×1) phase of the Ge(111) surface (Ichi-

kawa and Ino, 1980; Phaneuf and Webb, 1985). In the present section we try to clarify the experimental data on the basis of Monte Carlo calculations with the lattice gas model provided in the previous sections.

§§3.5.1 *Diffuse Scattering in the (1×1) Phase*

A diffraction pattern of electron from a surface gives us some information about the long-range order and also the short-range order in the surface. Especially in the surface with no long-range order, i.e., in the disordered phase of the surface it gives some important information on the short-range correlation of adatoms on the surface. The correlation function in the momentum space of the lattice gas model whose particles correspond to adatoms corresponds to the diffraction pattern of electron within the kinematical approximation. In the present subsection we discuss the temperature evolution of the system in the (1×1) phase with an attention focused upon the correlation function in the reciprocal space.

Figure 3.9 shows the temperature evolution of the calculated diffuse scattering patterns in the (1×1) phase for V_3/V_2=0.32 and V_6/V_2=0.1 where the ordered state is c(2×8). In the figures the integral-order Bragg spots whose intensities are far stronger than those of the fractional-order ones are not drown. Diffuse spots around the (2×2) superlattice Bragg points with strong intensity and distinctly split peaks appear immediately above the transition temperature as is shown in Fig. 3.9a. Relatively weak peaks at the (2×2) superlattice Bragg points are also reproduced. The

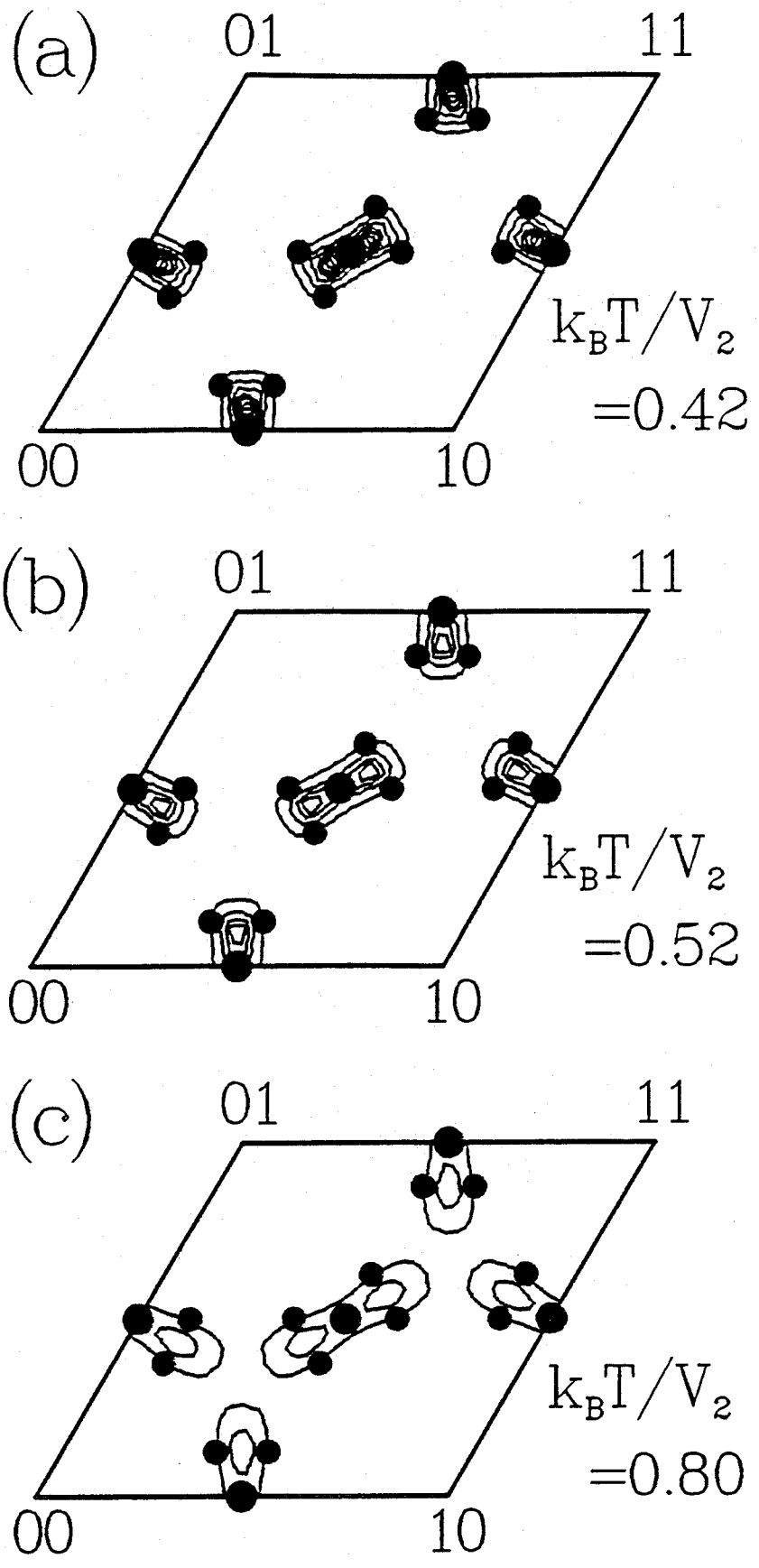

Figure caption on next page.

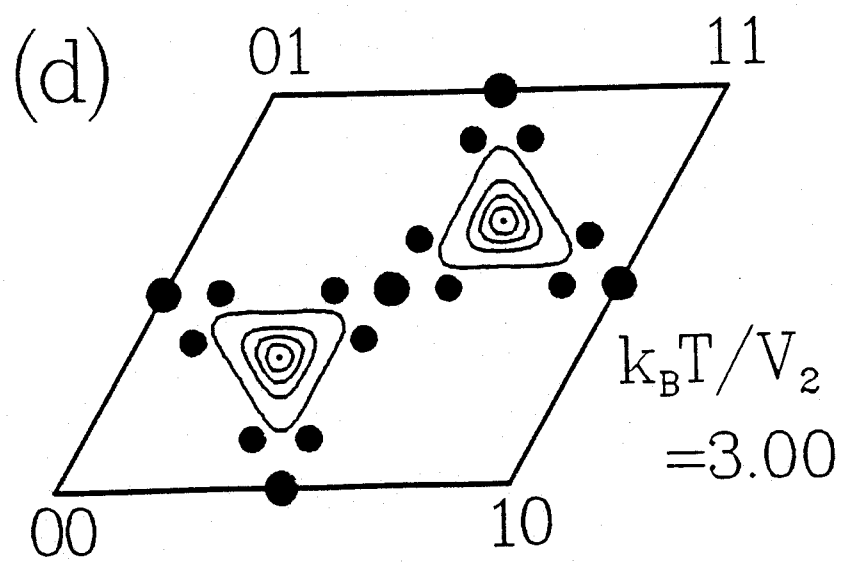

Figure 3.9
Calculated diffuse scattering patterns at various temperatures. V_3/V_2 = 0.32, V_6/V_2=0.1, N=48×48, and x=143/576 are assumed. The c(2×8) superlattice Bragg points are also shown by filled circles.

peak height of the spots decreases with temperature, and at the same time their positions move away toward the $(\sqrt{3} \times \sqrt{3})$ superlattice Bragg points; we notice that the positions of the peaks move continuously with temperature. With a further increase of temperature the spots fade away once at a temperature and reappear as diffuse spots around the $(\sqrt{3} \times \sqrt{3})$ superlattice Bragg points at higher temperatures. Except for the reappearance of diffuse spots around the $(\sqrt{3} \times \sqrt{3})$ superlattice Bragg points at high temperatures the calculated temperature evolution agrees with the observed one (Phaneuf and Webb, 1985).

We mention about the case where the ordered state is either the (2×2) or the c(2×4) briefly. In the case where the ordered state is the (2×2) one the essential feature in the (1×1) phase remains the same as in the above-mentioned case where the ordered state is the c(2×8), though the diffuse spots around the (2×2)

superlattice Bragg points just above the transition are too diffuse to show any distinct split peaks. On the other side, in the case where the ordered state is the c(2×4) one the situation is quite different; diffuse spots around the c(2×4) superlattice Bragg points appear immediately above the transition, they move away toward the $(\sqrt{3} \times \sqrt{3})$ superlattice Bragg points with temperature, and finally the diffuse spots around the $(\sqrt{3} \times \sqrt{3})$ superlattice Bragg points appear at sufficiently high temperatures. As can be seen from this, the (1×1) state for a set of interaction parameters with which the ordered state is the c(2×4) is not appropriate for discussing the reconstruction of Ge(111) at finite temperatures. This is the reason why we have chosen not three-particle interaction U_2 but the sixth neighbour pairwise one V_6 as a representative which causes the repulsive interaction between adjacent walls.

Diffuse spots around the $(\sqrt{3}\times\sqrt{3})$ superlattice Bragg points are observed in the (1×1) phase of the Si(111) surface by the RHEED and LEED experiments (Ino, 1977; Iwasaki *et al.*, 1987). As is discussed in §§3.5.2, the $(\sqrt{3}\times\sqrt{3})$ short-range order that the present model shows at sufficiently high temperatures is caused by the aggregation of triplets of mutually second neighbouring particles which play an important role in the gain of the entropy that is necessary in the (1×1) state. Although the existence of the stacking fault is characteristic of the (7×7) ordered arrangement of adatoms on the Si(111) surface, it is not compatible with the existence of the triplets (Kanamori, 1986). Therefore we can conjecture that the stacking fault disappears in the (1×1) phase of the Si(111) surface and that the present simple lattice gas model

is applicable in the (1×1) phase. In §4.3 the conjecture will be confirmed on the basis of the Monte Carlo calculation of another lattice gas model into which the Takayanagi mechanism stabilizing the (7×7) arrangement of adatoms is incorporated.

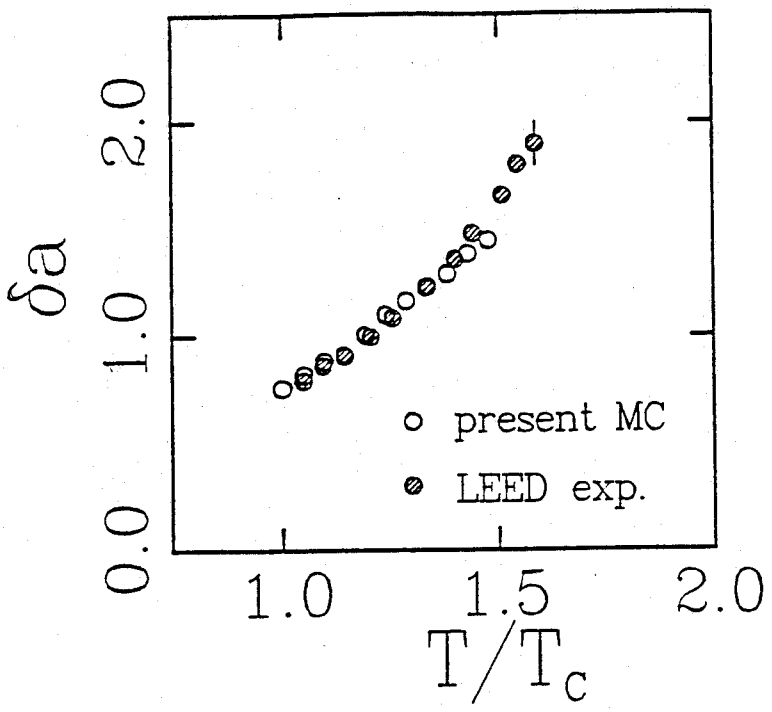

Figure 3.10
The temperature dependence of the splitting δ of diffuse spots around the (2×2) superlattice Bragg points. a and T_C denote the lattice constant of the triangular net and the transition temperature, respectively. Calculated splittings are shown by open circles. The experimental data after Phaneuf and Webb (1985) are shown by hatched circles for comparison. V_3/V_2=0.32, V_6/V_2=0.1, N=48×48, x=143/576, k_BT_C/V_2=0.42, T_C=300°C, and a=4.4Åare assumed.

Figure 3.10 shows the calculated temperature dependence of the splitting of the diffuse spots that appear around the (2×2) superlattice Bragg points for the case of V_3/V_2=0.32 and V_6/V_2=0.1. The splittings measured in the LEED experiment on the Ge(111) surface by Phaneuf and Webb (1985) are also indicated in the figure for comparison, where we assume k_BT_C/V_2=0.42 which is the

transition temperature of the present model, T_C=300°C, and the lattice constant of the Ge(111) surface a=4.4Åwhich corresponds to a unit lattice spacing of the triangular net of the model. We can see from the figure that both the splitting immediately above the transition and the temperature evolution of the splitting in the (1×1) phase can be reproduced well by the present lattice gas model. We note that the temperature evolutions of the calculated peak height and peak width agree qualitatively with those obtained in the experiments (Ichikawa and Ino, 1980; Phaneuf and Webb, 1985), as can be seen from Fig. 3.9. We have a quantitative disagreement between the experimental data; the diffuse peaks just above the transition observed in the RHEED experiment are sharper than ones in the LEED experiment. Therefore we have above confined ourselves only to comparing the calculated temperature dependence of the peak splitting with the experimental data.

§§*3.5.2 Domain Structure of Particle Arrangement*

One of the advantages of the simulation calculation is that it can give the snapshots of the particle arrangements, which would reveal the origin that the characteristic diffuse pattern immediately above the transition arises from.

We have found that the diffuse pattern immediately above the transition arises from the characteristic domain structure shown in Fig. 3.11a where particles keep one of the four kinds of the (2×2) arrangements in each domain. The walls separating the domains terminate either at triplets of mutually second neighboring

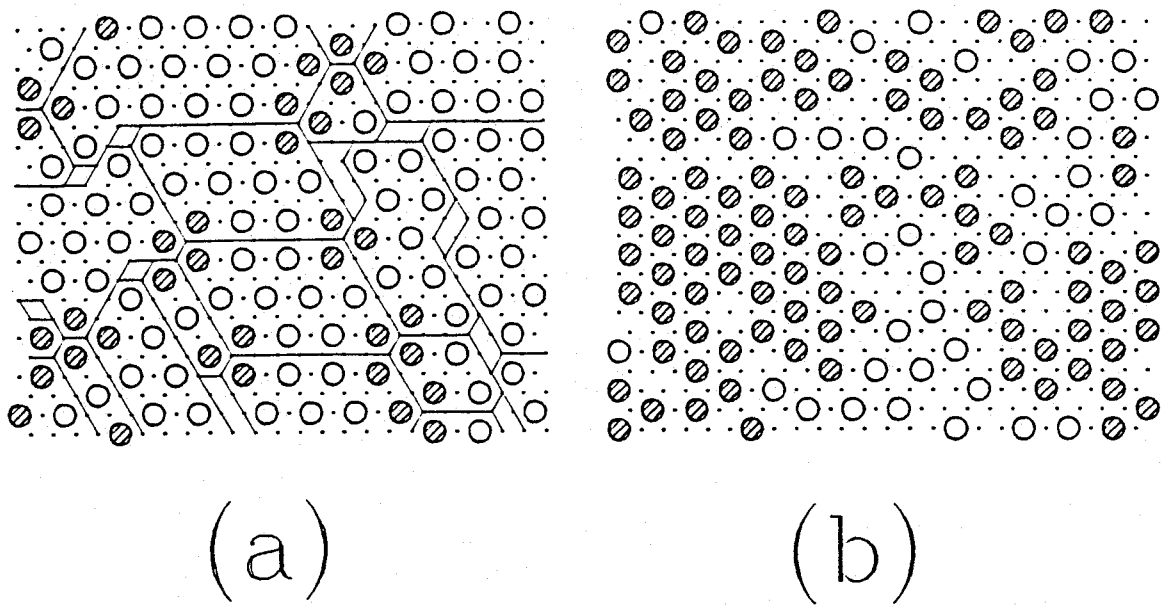

Figure 3.11
Typical particle arrangements (a) just above the transition (k_BT/V_2 = 0.42) and (b) at a sufficiently high temperature (k_BT/V_2=3) in the case of V_3/V_2=0.32 and V_6/V_2=0.1. Those particles which participate in mutually second neighbouring triplets are denoted by hatched circles. Walls which separate the particle arrangement into (2×2) domains are shown by lines.

particles or voids. Mean size of the domains corresponds to the splitting of the diffuse spots, while thermal fluctuation or in other words meandering of the domain walls makes the spots diffuse. The sharpness of the diffuse spots which is in agreement with experiment arises from the uniformity of the size of the domains. The wall interaction affects the domain structure above the transition. The sixth neighbour interaction plays a role to hinder the

formation of the smallest wall intervals and thus to make the size distribution of the domains uniform. In fact in the case without the sixth neighbour interaction the size distribution of domains is more broad to make the spots which appear around the (2×2) superlattice Bragg points in the reciprocal-space correlation function more diffuse. Phaneuf and Webb (1985) proposed two possible adatom arrangements which may correspond to the disordered state of Ge(111). The particle arrangement found in the present investigation is similar to one of them.

Triplets of mutually second neighboring particles make the local concentration near the triplets higher than that of the inside of the domains where the average concentration is kept. Thus the appearance of the triplets should be always accompanied by that of the voids. It is discussed in §§3.5.4 that the presence of the triplets and voids is essential to the entropy gain required for the high temperature (1×1) phase; in fact the entropy is shown to be given approximately by a universal function of the number of the triplets.

With increasing temperature the number of the triplets as well as the voids increases to make the mean size of the domains smaller; the splitting of the diffuse spots becomes larger accordingly. Finally the domain structure collapses and the triplets aggregate, giving rise to an apparent $(\sqrt{3} \times \sqrt{3})$ short-range order. Figure 3.11b gives a snapshot at this stage.

We have demonstrated that the present model can reproduce the essential feature of the temperature evolution of the Ge(111) and clarified the origin from which the feature arises for

just a choice of a set of parameters. We stress, however, that the qualitative feature is not dependent on the choice of the parameters; the choice affects only quantitative aspects of the splitting just above the transition and the temperature dependence of the splitting. Therefore we are able to say that the characteristic feature of Ge(111) in the (1×1) phase can be understood from a general statistical-mechanical behaviour of a system of lattice gases which correspond to adatoms situated at the energetically favourable sites on the surface.

§§3.5.3 *Underlying Mechanism of the Characteristic Domain Structure*

We discuss the mechanism underlying the appearance of the above-mentioned domain structure in the (1×1) phase of the present lattice gas model.

The wall vertices corresponding to the triplets of mutually second neighbouring particles and voids have a positive energy which forbids them to appear in the ordered state. As is discussed in §§3.5.4, the triplets and also the voids play an important role for the entropy gain required in the (1×1) state. Above the transition temperature the entropy gain makes the free energy of the vertices negative. The wall energy is negative in the case where the ordered state is the c(2×8); while for the ordered state of (2×2) the wall energy is positive, but the free energy of the walls which should be accompanied by mutually second neighbour triplets and voids is probably negative in the (1×1) state. It is known that a honeycomb network of the walls is favoured as the ground state if

both the wall energy and the wall vertex energy are negative (Bak *et al.*, 1979). In the present case the thermal fluctuation forces the walls to meander. Thus it is understandable that the domain structure above the transition corresponds to a deformed network of the walls.

§§3.5.4 Entropy

Kanamori (1986) conjectured previously that the entropy of the present lattice gas system in the (1×1) state is mainly contributed by triplets of mutually second neighbouring particles. In the state without the triplets, X_1=0, the system have no entropy, since each particle cannot move freely; the entropy of the system takes the value of the order of magnitude of $k_B\sqrt{N}$ at most. While the finite $\langle X_1 \rangle$ produces room for the movement of the particles; then the system has a finite entropy. And the larger the number of the triplets is, the more the entropy of the system. Thus the entropy of the present system is closely related with the number of the triplets. In this section we clarify the relation between the entropy of the system and the number of triplets of mutually second neighbouring particles on the basis of the present Monte Carlo calculations.

We estimate the entropy at finite temperatures from the present Monte Carlo data with the use of the method proposed by Binder (1981). The entropy of the system S at a temperature T is given by

$$S = S_\infty - \int_{\langle E \rangle_T}^{\langle E \rangle_\infty} \frac{\mathrm{d}\langle E \rangle}{T}, \qquad (3.10)$$

or

$$\frac{S}{Nxk_{\rm B}} = \frac{S_\infty}{Nxk_{\rm B}} - \int_{\langle E\rangle_T/NxV_2}^{\langle E\rangle_\infty/NxV_2} \frac{{\rm d}\varepsilon}{k_{\rm B}T/V_2},$$
$$\varepsilon = \frac{\langle E\rangle}{NxV_2}, \tag{3.11}$$

where S_∞ and $\langle E\rangle_\infty$ denote the entropy and the energy of the system at the high temperature limit $T = +\infty$, respectively, and ${\rm d}\langle E\rangle$ is defined by

$${\rm d}\langle E\rangle = C(T){\rm d}T \tag{3.12}$$

with the specific heat of the system $C(T)$ at a temperature T. The integration in eq. 3.11 has been evaluated, interpolating by linear functions the derivatives of the integrand in the equation at some temperatures sufficient to obtain values of the entropy with the accuracy which is necessary for the present discussion.

	L=24	L=48
$\langle p_2\rangle_\infty/Nx$	1.783 ± 0.008	1.789 ± 0.002
$\langle p_3\rangle_\infty/Nx$	0.375 ± 0.007	0.371 ± 0.002
$\langle p_6\rangle_\infty/Nx$	1.349 ± 0.018	1.365 ± 0.005
$\langle X_1\rangle_\infty/Nx$	0.840 ± 0.007	0.847 ± 0.002

Table 3.1
The numbers of second, third, and sixth neighbouring pairs of particles and that of triplets of mutually second neighbouring particles at the infinite temperature. The linear system sizes L=24 and 48 are assumed.

The Monte Carlo data for the energy of the system and the number of the triplets at the infinite temperature $\langle E\rangle_\infty$ and

$\langle X_1 \rangle_\infty$ are necessary for the estimate of the entropy of the system. Table 3.1 presents the numbers of pairs of particles $\langle p_2 \rangle_\infty$, $\langle p_3 \rangle_\infty$, and $\langle p_6 \rangle_\infty$ and that of triplets $\langle X_1 \rangle_\infty$ at $T=+\infty$. The energy of the system at the infinite temperature is evaluated, putting these values $\langle p_2 \rangle_\infty$, $\langle p_3 \rangle_\infty$, and $\langle p_6 \rangle_\infty$ for $\langle p_2 \rangle$, $\langle p_3 \rangle$, and $\langle p_6 \rangle$, respectively, in eq. 3.9. We have obtained these values from calculations where particles of the system are assumed not to interact with each other except for the hard hexagon condition $V_1=+\infty$. In the calculations the ensemble averages have been taken over 10 000 and 20 000 Monte Carlo steps for linear system sizes of $L=24$ and 48, respectively.

Figure 3.12 shows the calculated entropy vs. $\langle X_1 \rangle$ relation for various sets of interaction parameters in each case of which the ordered state is either the (2×2), c(2×4), or c(2×8) state. This shows clearly that the entropy of the system is given approximately by a universal function of the number of the triplets which is independent of the choice of a set of the interaction parameters except for the case of $V_3/V_2=0.8$ and $V_6=0$; some additional effect probably works in the exceptional case where the set of interaction parameters is situated in the parameter space near the parameter region with no ordered ground state as is seen from Fig. 3.4. Thus the present investigation has assured us of the conjecture previously discussed by Kanamori.

Finally we note that we can conclude from the above discussion that the following relation holds independently of the choice of values of the interaction parameters, i.e., independently of the

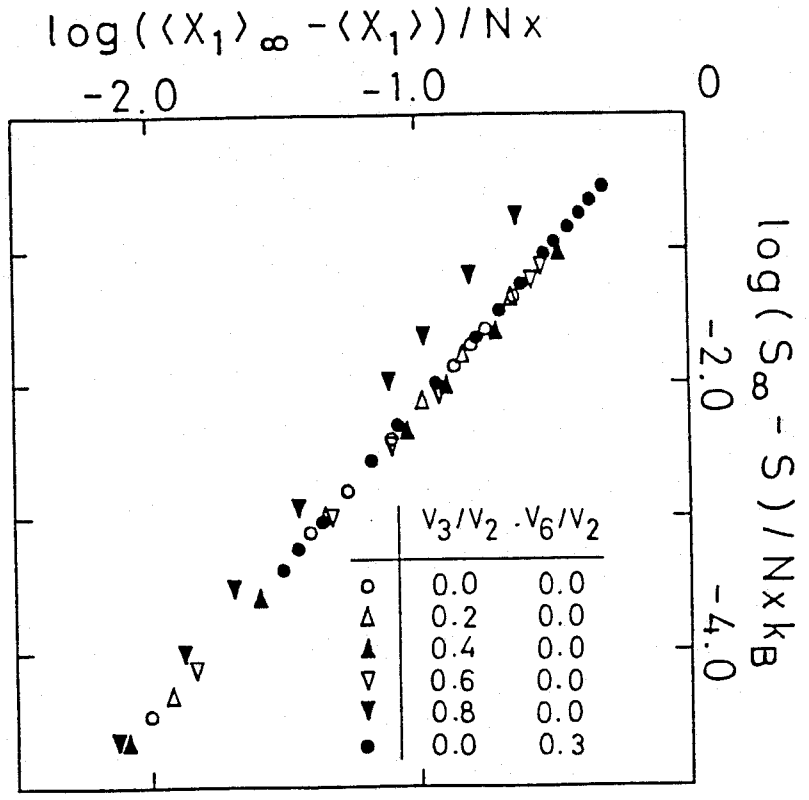

Figure 3.12
Entropy S vs. the number of triplets of mutually second neighbouring particles $\langle X_1 \rangle$. S_∞ and $\langle X_1 \rangle_\infty$ denote the entropy and the number of the triplets, respectively, at the infinite temperature.

ordered state of the system:

$$S_\infty - S \propto [\langle X_1 \rangle_\infty - \langle X_1 \rangle]^\alpha. \tag{3.13}$$

The exponent α takes the value $\alpha \sim 2.3$ except for the exceptional case of V_3/V_2=0.8 and V_6=0 where α=2.64±0.01.

CHAPTER IV

Extended Lattice Gas Model: Si(111) Case

In the present chapter we introduce a lattice gas model modified in a way that the essential part of the Takayanagi mechanism which stabilizes the (7×7) state as the ground state is incorporated, and carry out the Monte Carlo calculation to discuss the reconstruction of the Si(111) surface at finite temperatures. In §4.1 the model is presented, stressing the relation with the Si(111) surface. The ground states of the model is also analyzed. Section 4.2 describes the computational method used in the following Monte Carlo calculation in detail. In the next section, §4.3, the Monte Carlo calculation is presented. It is shown that the model reproduces the feature observed in experiments on the surface both below and above the transition. The disappearance of stacking faults in the (1×1) phase is also discussed on the basis of the calculation. A part of the discussion presented in this chapter has been published (Kanamori and Sakamoto, 1991; Sakamoto and Kanamori, 1991).

§4.1 An Extended Lattice Gas Model for the Takayanagi Reconstruction

As is mentioned in §2.2, the (7×7) arrangement of Si(111) below the transition temperature cannot be of the lowest energy of a simple lattice gas model applicable to Ge(111). This gives a theoretical support to the fact that the (7×7) arrangement of adatoms takes the structure with the dimer formation and the stacking fault in the substratum layers.

One of ways to discuss the phase transition and the (1×1) phase of the surface theoretically is to make an investigation of a lattice gas model modified in such a way that the stabilizing mechanism of the Takayanagi model is incorporated. In the model we distinguish between two kinds of particles each of which corresponds to an adatom on a normal or a stacking-faulted substratum layer; the available sites for them are assumed to make a triangular net. The effect to stabilize the structure through the dimer formation itself is introduced into the model as appropriate values of the interaction energy between different sorts of particles at the second neighbour sites; as is discussed in detail below, the second neighbour interaction between such particles is of threefold symmetry.

§§*4.1.1 Model*

The Takayanagi model stabilizes the adatom arrangement observed in the Si(111) surface essentially by the dimer formation in the second underlayer of the surface. So as to form dimers

it is necessary that the surface should be accompanied by both stacking-faulted regions and normal ones in the surface layer, i.e., in the first underlayer. Although the stacking fault raises the surface energy to some extent, the dimer formation stabilizes the structure of the surface sufficiently. Thus we have to give each particle of the lattice gas model with which we discuss the Si(111) surface an attribution indicating whether the particle corresponds to an adatom on a normal substratum layer or on a stacking-faulted one. In other words, we may regard each particle as one which possesses such an internal degree of freedom as the Ising psudospin. Moreover, the available sites for particles of the model are assumed to make a triangular net, since the adatom arrangement of the surface can be described as a particle arrangement on a triangular lattice. In addition we assume that the concentration of particles is 12/49 which corresponds to that of adatoms on the surface in the (7×7) state.

We may represent the particles by equilateral triangles whose vertices correspond to substratum atoms making bonds with the corresponding adatoms. There are two possible orientations of the triangles corresponding to the choice of normal or stacking faulted substratum. Figure 4.1 shows the particle arrangement corresponding to the (7×7) state of the Si(111) surface as an example of the representation. The comparison with Fig. 2.1 which displays the (7×7) DAS structure will make the definition of the triangles transparent. Figure 4.2 shows more examples of the representation.

We assume that the interaction between particles is ex-

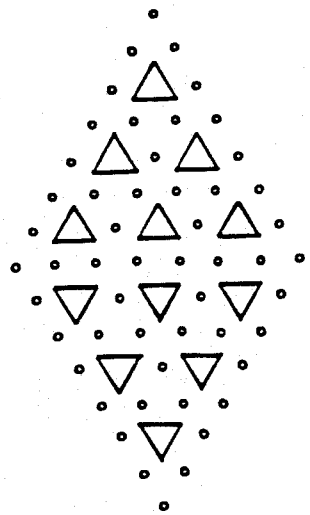

Figure 4.1
The (7×7) arrangement of triangles. A unit cell is shown.

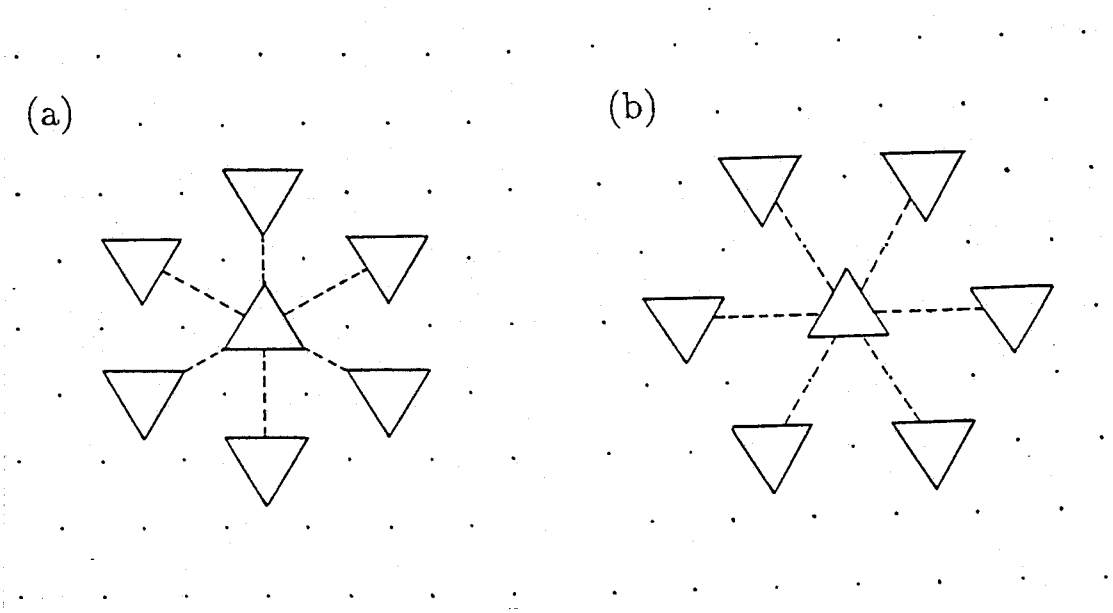

Figure 4.2
Triangles of different orientations at (a) second and (b) third neighbour sites.

tended up to the third neighbour sites on a triangular net. The third neighbour interaction is necessary for the appearance of the (7×7) state as the ground state, as is discussed in the next subsection §§4.1.2. The energy of the model is represented by

$$E = \delta\mu N^{\text{s.f.}} + V_1 p_1 + \bar{V}_1 \bar{p}_1 + V_2 p_2 + \bar{V}_2 \bar{p}_2 + \bar{V}_2' \bar{p}_2' + V_3 p_3 + \bar{V}_3 \bar{p}_3, \quad (4.1)$$

where p_k and $\bar{p}_k$ (and $\bar{p}_2'$) denote the number of the k-th neighboring pairs of the same and different triangles, respectively; V_k and $\bar{V}_k$ (and $\bar{V}_2'$) denote the interaction energy of the corresponding pairs of particles, i.e., triangles; $\delta\mu$ is the chemical potential difference between particles corresponding to adatoms on the normal and stacking-faulted substratum layer, which corresponds to the energy increase per particle by producing stacking faults in the substratum; and $N^{\text{s.f.}}$ is the number of particles corresponding to adatoms on the stacking-faulted substratum.

Two adatoms on the surface corresponding to a nearest neighbouring pair of triangles of the same orientation which have to share a dangling bond of an atom in the substratum will have a sufficiently repulsive interaction; we assume $V_1 = +\infty$. Since two adatoms which correspond to a nearest neighbouring pair of different triangles make substratum atoms too close, the pair is also forbidden energetically ($\bar{V}_1 = +\infty$). The second neighbour interaction of triangles of the same orientation is assumed to be repulsive, since the $(\sqrt{3} \times \sqrt{3})$ arrangement of adatoms does not appear as the ordered state of the surface; we use hereafter the interaction energy $V_2 > 0$ as units by which the energy and the temperature of the system are measured. We distinguish between two kinds of

second neighbouring pairs of triangles of different orientations, the numbers of which are denoted by $\bar{p}_2$ and $\bar{p}_2'$, and their interaction constants $\bar{V}_2$ and $\bar{V}_2'$ by the directions of the pairs. In one of them the line connecting the two particles passes vertices of the triangles pointing to each other, and in the other the line passes the facing edges, as is illustrated in Fig. 4.2a. The first case is forbidden, since the substratum atoms come too close to each other; we assume the corresponding interaction energy $\bar{V}_2'=+\infty$. While pairs in the second case are found in a discommensuration wall where a chain of dimers in the Takayanagi model is generated. The pairs should lower the wall energy sufficiently to stabilize the (7×7) arrangement as the ground state; the condition is $\bar{V}_2 < V_2$. Thus the interaction between triangles of different orientations at the second neighbour sites is of threefold symmetry. We notice that the state where the Takayanagi walls run parallel cannot be allowed in the present model because of $\bar{V}_2' = +\infty$; the c(2×4) state which is one of the ground states of the model is made of just a kind of triangles. Furthermore we assume that the interaction between triangles of different orientations at third neighbour sites is sufficiently repulsive but finite. Figure 4.2b shows examples of the associated pairs. The atom which is a bonding mate of adatoms corresponding to the pair has a dangling bond, and the situation makes the pair energetically unfavourable. Finally we mention about the third neighbour interaction energy of triangles of the same orientation V_3 and the energy increase per adatom by producing a stacking faulted substratum $\delta\mu$. The third neighbour interaction energy is used as an adjustable parameter in calculations; the strength of

it determines the ground state of the model which corresponds either to the (7×7), (2×2), or c(2×4) arrangement of particles. The energy increase $\delta\mu$ is assumed to be positive but not too large to stabilize the (7×7) arrangement as the ground state. The choice of the values of them in calculations is mentioned in §4.3.

We have assumed above $V_1=\bar{V}_1=\bar{V}_2'=+\infty$, or $p_1=\bar{p}_1=\bar{p}_2'=0$. We notice that the hard hexagon condition $p_1=\bar{p}_1=0$ holds in the present model which ensure the $(\sqrt{3}\times\sqrt{3})$ short-range order at sufficiently high temperatures. Thus the energy of the model E given by eq. 4.1 is reduced to

$$E = \delta\mu N^{\text{s.f.}} + V_2 p_2 + \bar{V}_2\bar{p}_2 + V_3 p_3 + \bar{V}_3\bar{p}_3. \qquad (4.2)$$

Then the ensemble average of the energy $\langle E\rangle$ is evaluated from the following expression:

$$\langle E\rangle = \delta\mu\langle N^{\text{s.f.}}\rangle + V_2\langle p_2\rangle + \bar{V}_2\langle\bar{p}_2\rangle + V_3\langle p_3\rangle + \bar{V}_3\langle\bar{p}_3\rangle. \qquad (4.3)$$

We have assumed that $\bar{V}_3$ is sufficiently large. Since the value of $\bar{V}_3$ is not essential to the discussion of the reconstruction of Si(111), we assume rather arbitrarily $\bar{V}_3/V_2=2.0$ in the Monte Carlo calculations presented in the following section. We notice that we thus have three adjustable parameters $\bar{V}_2/V_2$, V_3/V_2, and $\delta\mu/V_2$ in the calculations.

§§*4.1.2 Ground States of the Model*

We consider the lowest-energy state of the extended lattice gas model presented above. If the triangles are all in the same orientation, the model reduces to the simple lattice gas model. In

the following we confine ourselves for simplicity to the states of the simple lattice gas model and the $(n \times n)$ states composed by triangles of different orientations.

We can regard the (2×2) state as that corresponding to the $(n \times n)$ state of the Takayanagi model with infinitely large n. Since the energy of the $(n \times n)$ state of the present model varies monotonically with n, the lowest energy state of the $(n \times n)$ ones is either the (2×2) state or the $(n \times n)$ one with the smallest n that is allowed in the model. The (3×3) and (5×5) states cannot appear as the ground state of the model, since we assume in the model that the concentration of particles is 12/49; thus the $(n \times n)$ state with the smallest n is the (7×7) one. As has been mentioned in §3.2, the lowest-energy state of the simple lattice gas model with up to the third neighbour interaction is either the (2×2) state or the c(2×4) one. Thus the ground state of the present lattice gas model is the lowest-energy one of the (7×7), (2×2), and c(2×4) ones so far as we assume the condition X_1=0.

The energy of the system in the (7×7) state $E_{7\times7}$ is represented by

$$E_{7\times7} = \{\frac{1}{2}\delta\mu + \frac{3}{4}\bar{V}_2 + \frac{3}{2}V_3\}Nx, \tag{4.4}$$

where N and x denote the number of lattice sites and the concentration of particles, respectively. The energies in the (2×2) and c(2×4) states, $E_{2\times2}$ and $E_{2\times4}$, are written as

$$E_{2\times2} = 3V_3Nx, \tag{4.5}$$

and

$$E_{2\times4} = \{V_2 + V_3\}Nx, \tag{4.6}$$

respectively. Dividing the parameter space into two regions makes the analysis of the ground state easy. In the case that the wall energy $w = (1/2)V_2 - V_3$ is positive the lowest energy state is either the (2×2) one or the (7×7) one, and in the other case ($w < 0$) that can be either the c(2×4) or the (7×7) with the condition X_1=0. In the former case, if $E_{7\times7} > E_{2\times2}$, i.e., $V_3 < (1/3)\delta\mu + (1/2)\bar{V}_2$, the (2×2) state is of the lowest energy; otherwise the lowest energy state is the (7×7) one. In the latter case of the negative wall energy, $V_3 > -\delta\mu + 2V_2 - (3/2)\bar{V}_2$ makes the c(2×4) state of the lowest energy with the condition X_1=0 that is satisfied for $V_3 < V_2$, and with $V_3 < -\delta\mu + 2V_2 - (3/2)\bar{V}_2$ and X_1=0 the (7×7) state is the lowest energy one. We note that for the positive but not too large value of $\delta\mu$ we have the parameter region where the (7×7) state appears as the ground state. In the region, although the energy of the system is raised by producing stacking faults, the Takayanagi walls lower the energy of the system sufficiently to stabilize the (7×7) state.

Figure 4.3 shows the ground-state phase diagram for the case of $\delta\mu$=0. We can see from the figure that the condition the Takayanagi model is stabilized is $\bar{V}_2 < V_2$.

§4.2 Details of the Calculation Method

In this chapter we carry out Monte Carlo calculations of the present extended lattice gas model at finite temperatures with canonical ensembles, fixing the total number of particles in the model. We have described in detail in §3.3 the calculation method for the simple lattice gas model applicable to Ge(111). The essen-

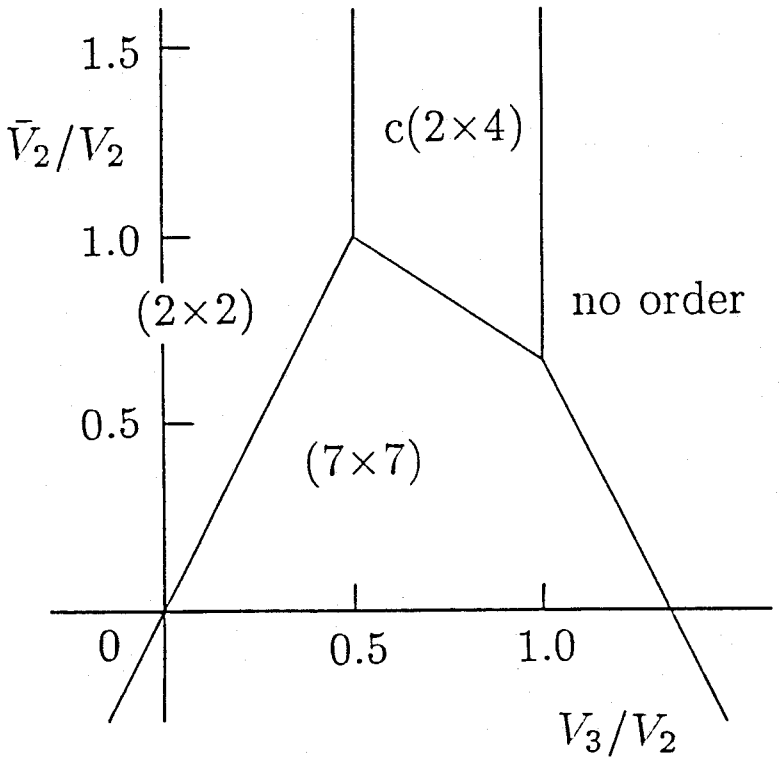

Figure 4.3
Ground-state phase diagram of the extended lattice gas model. $\delta\mu$=0 is assumed.

tial part of the method for the present extended model is the same as that in the simple model case. In the present section we describe the calculation method briefly, focusing our attention upon the difference from that in the previous case.

§§4.2.1 System Size, Particle Number, and Boundary Condition

Each calculation presented in this chapter is carried out with a system of a finite size. We assume the lattice sizes of 28×28 and 56×56 sites. These system sizes are sufficient to discuss the problem of the Si(111) surface, since the characteristic correlation length of the system is probably shorter than the linear sizes we

adopt. So as to eliminate the boundary effect from the calculations, we use lattices with periodic boundary conditions.

As is discussed in the previous section, we consider the system whose concentration of particles x is 12/49. Adopting x=12/49 precisely, however, we should have the same difficulty as in the previous simple lattice gas model case. Therefore we assume in the calculations that the concentration of particles is 191/784 which is slightly less than 12/49.

In order to fix the total number of particles we use an *a priori* probability similar to the one for the case of the simple lattice gas model. Because we have two kinds of particles in the present extended model, we have to incorporate into the transition probability the process that a triangle changes its orientation in a Monte Carlo trial in addition to the process of moving a particle to one of its nearest neighbour sites. Thus we assume in the present calculations that $P_{cc'} \neq 0$ if a configuration c' is one caused by either moving a particle of the system with a configuration c to one of the nearest neighbour lattice sites or changing the sort of the particle, and that $P_{cc'} = 0$ for other cases. The *a priori* probability by which a given particle changes to the other sort of one is assumed to be $(2/8)(1/Nx)$, and that for moving to one of its nearest neighbour sites is to be $(1/8)(1/Nx)$. This choice of an *a priori* probability is convenient for a calculation; because we use a sequence of integral random numbers in the calculation, we can generate the probability by taking three bits of a random number.

§§4.2.2 Correlation Function Calculation

In order to demonstrate that the present extended lattice gas model can reproduce the (1×1) state of the Si(111) surface we calculate the correlation function $S(k)$ of the present model in the momentum space which is defined by the same equation as in the case of the simple lattice gas model, eq. 3.6. In the equation we do not distinguish between two sorts of particles; if the site r is occupied by a particle, the occupation number $n(r)$ in the equation takes the value of unity independently of the kind of the particle.

In the calculation of the function $S(k)$ for the previous simple model case we took an average over three independent directions which correspond to rotating a configuration by 0, $2\pi/3$, and $4\pi/3$, respectively, around a lattice site. In the present extended model case we also take an average over the three directions in the evaluation of $S(k)$.

§4.3 Phase Transitions and the (1×1) Phase

In this section we carry out the Monte Carlo calculation of the lattice gas model for the Takayanagi reconstruction presented in the previous section in order to discuss the Si(111) surface at finite temperatures. In §§4.3.1 and §§4.3.2 it is demonstrated that the model can reproduce the phase transition and the diffuse scatterings of electron in the (1×1) phase. We discuss the disappearance of the stacking fault in the (1×1) phase in §§4.3.3.

§§4.3.1 Phase Transitions

It is not clear whether or not the phase transition between

the ordered state and the disordered one occurs in the present model. We first have to confirm this point to discuss the reconstruction of the Si(111) surface with the model.

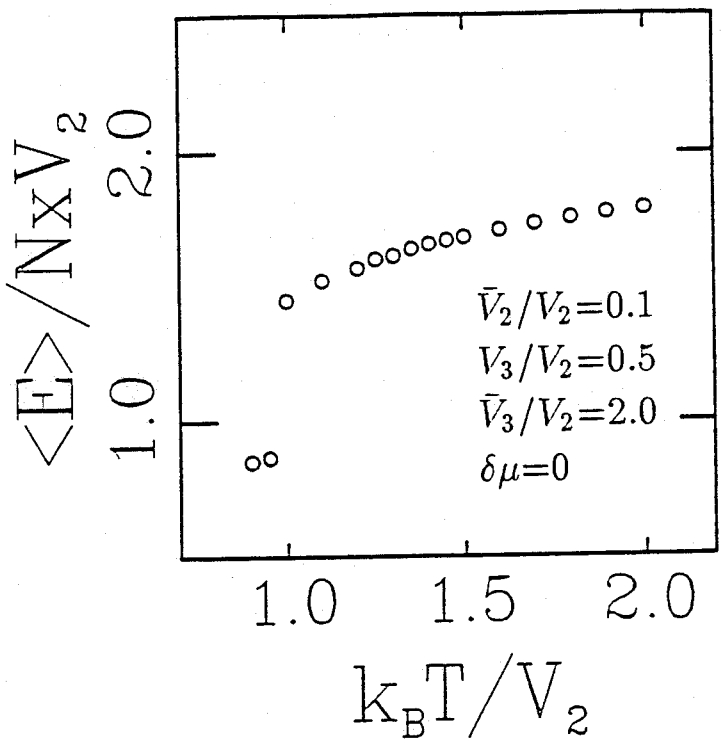

Figure 4.4
The temperature dependence of the energy for $\bar{V}_2/V_2$=0.1, V_3/V_2=0.5, and $\delta\mu$=0.

Figure 4.4 shows an example of the calculated temperature dependence of the energy for the case of $\bar{V}_2/V_2$=0.1, V_3/V_2=0.5, and $\delta\mu$=0 where the ordered state is the (7×7) one. Ensemble averages were taken over 100 000 Monte Carlo steps in the calculations. The lattice with 56×56 sites is assumed there. This clearly indicates the occurrence of the first-order phase transition between the disordered (1×1) state and the (7×7) state. The energy vs. temperature relation has been obtained from calculations with increasing temperature. The transition from the disordered

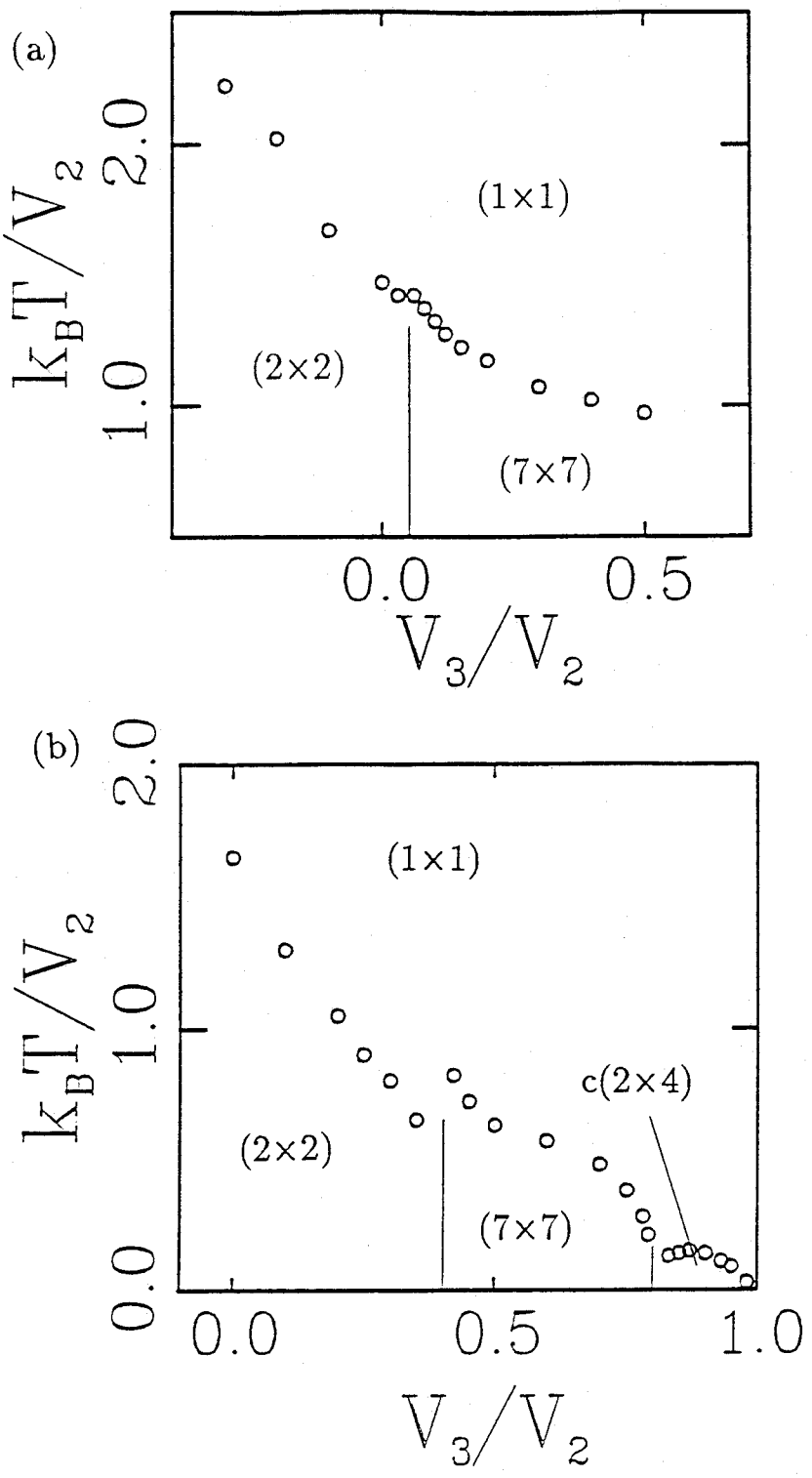

Figure 4.5
Phase diagrams in the T vs. V_3 plane for (a) $\bar{V}_2/V_2$=0.1 and (b) 0.8. $\delta\mu$=0 is assumed.

(1×1) state to the ordered (7×7) one has not taken place in the present calculations due to the complicated ordered structure and

the local updating of the configuration in the Monte Carlo scheme. A system of a smaller size with 14×14 lattice sites, however, transforms reversibly both from the (7×7) state to the (1×1) and from the (1×1) to the (7×7).

Though we have above presented just an example, the feature of the phase transition is independent of the choice of a parameter set. Figure 4.5 shows the phase diagrams in the T-V_3 plane for the cases of $\bar{V}_2/V_2$=0.1 and 0.8, where $\delta\mu$=0 is assumed. In the case of $\bar{V}_2/V_2$=0.1 the ordered state of the model is the (2×2) state for $V_3/V_2 < 0.05$ and the (7×7) one for $0.05 < V_3/V_2$. While in the case of $\bar{V}_2/V_2$=0.8 the c(2×4) state appears as the ground state; the ground state of the model is the (2×2), (7×7), and c(2×4) states for $V_3/V_2 < 0.4$, $0.4 < V_3/V_2 < 0.8$, and $0.8 < V_3/V_2 < 1$, respectively. For the values of the interaction parameters where the ordered state is either the (2×2) or c(2×4) state the present extended model is reduced to the simple lattice gas model with up to the third neighbour interaction so far as the ordered state is concerned. The phase transition from each of the ordered states (7×7), (2×2), and c(2×4) to the (1×1) state is of the first kind.

§§4.3.2 *Diffuse Scatterings Just above the Transition*

Figure 4.6 shows the calculated diffuse scattering patters just above the transitions for various values of the third neighbour interaction energy V_3 with which the ordered state is the (7×7) one; $\bar{V}_2/V_2$=0.1 and $\delta\mu$=0 are assumed. Each calculation was continued to 200 000 Monte Carlo steps because of a large fluctuation in the configuration space. For the cases of large values of V_3/V_2

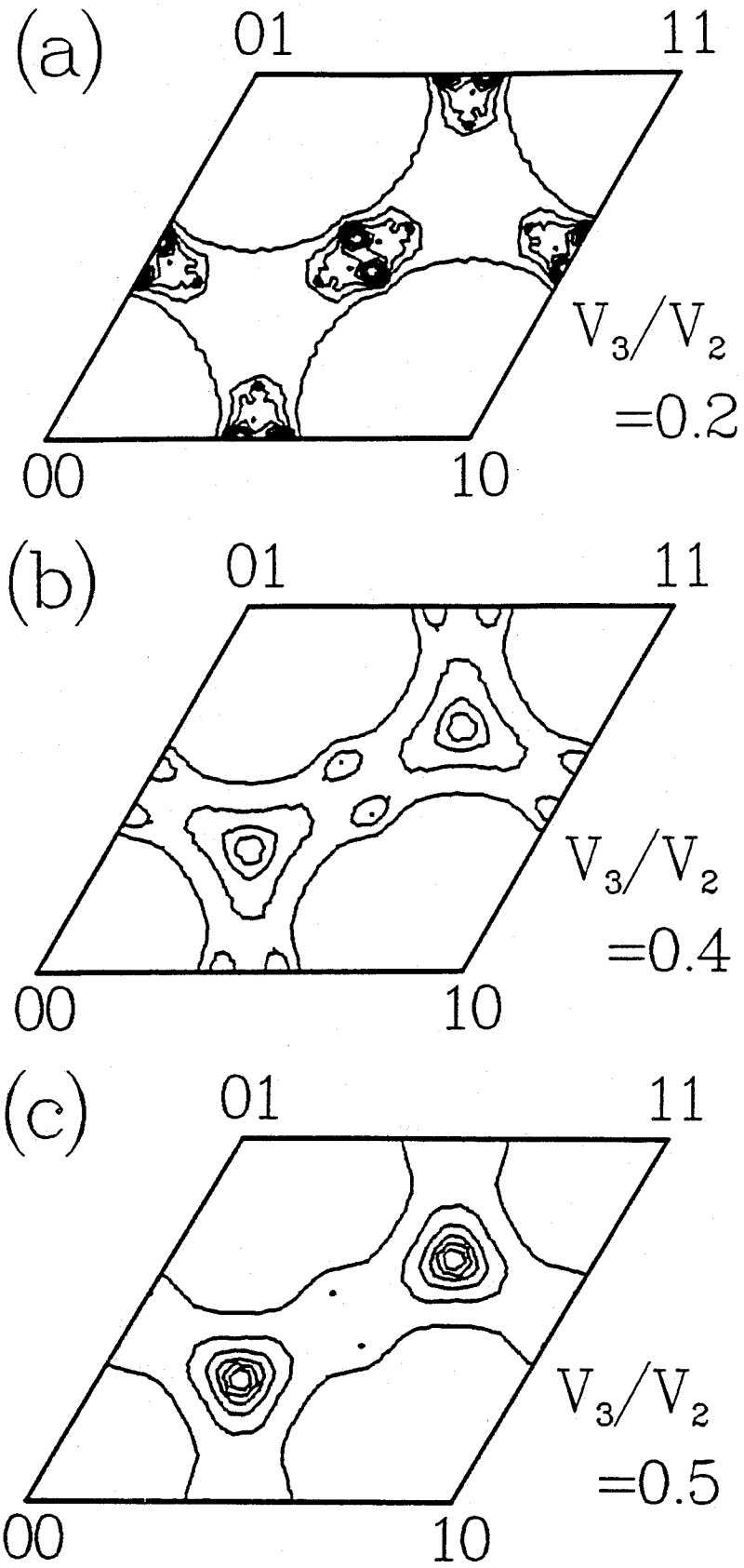

Figure 4.6
Diffuse scattering patterns immediately above the transitions for various values of V_3. $\bar{V}_2/V_2$=0.1 and $\delta\mu$=0 are assumed.

the $(\sqrt{3}\times\sqrt{3})$ diffuse spots which are observed in the RHEED and LEED experiments on the (1×1) state of the Si(111) surface are reproduced. Thus it has been clarified that the present model with appropriate sets of interaction parameters is capable of describing well the surface reconstruction of Si(111) in the whole range of the temperature both below and above the transition.

As is mentioned above, the large value of V_3 yields diffuse spots around the $(\sqrt{3}\times\sqrt{3})$ Bragg points immediately above the transition, which is in agreement with experiments. The following two mechanisms give an explanation of this result. The large value of V_3 raises the energy of the (1×1) state divided by (2×2) domains in which particles show one of the four (2×2) arrangements found in the investigation on Ge(111) presented in §3.5, and favours the more disordered state which gives rise to the $(\sqrt{3}\times\sqrt{3})$ diffuse spots. Also the Takayanagi mechanism which is incorporated in the present model stabilizes the ordered state, raising the transition temperature to skip the temperature range of the (1×1) state of the Ge(111) type; the Takayanagi mechanism plays an important role in producing the diffuse spots around the $(\sqrt{3}\times\sqrt{3})$ superlattice Bragg points just above the transition.

§§*4.3.3 Disappearance of Stacking Faults in the (1×1) Phase*

The existence of triplets of mutually second neighbouring particles is essential to the (1×1) state of the surface for the entropy gain necessary there. It is not, however, compatible with that of both normal and stacking faulted regions in the surface layer. With this reasoning Kanamori (1986) conjectured that the

stacking fault should disappear in the (1×1) phase of the Si(111) surface and that the simple lattice gas model is there applicable. The conjecture has not been confirmed experimentally as yet. Since our aim is to construct a model capable of reproducing the evolution of the surface in the whole temperature range without making *ad hoc* assumptions for each phase, it is an important problem to examine whether the stacking faults will persist in the (1×1) phase or not. In the present subsection we try to confirm the conjecture theoretically on the basis of the Monte Carlo calculation of the present extended lattice gas model.

Figure 4.7 shows the temperature dependence of the number of particles which correspond to adatoms on the normal substratum layer $N^{\mathrm{normal}}=Nx - N^{\mathrm{s.f.}}$ for the cases of $\delta\mu/V_2=0$ and 0.5; $\bar{V}_2/V_2=0.1$ and $V_3/V_2=0.5$ where the ordered state is the (7×7) are assumed. Ensemble averages were taken over 100 000 Monte Carlo steps in the calculations. The lattice with 56×56 sites is assumed there. In the figure the increase of the number of particles corresponding to the normal substratum in the (1×1) phase clearly indicated even for the case of $\delta\mu=0$. We note that the increase of N^{normal} in this case is caused only by the entropy gain necessary in the (1×1) phase. If we assume the finite energy increase by producing the stacking faulted substratum, the imbalance between the numbers of particles corresponding to normal and stacking-faulted substratum layers will be more distinct. In fact, the calculation for $\delta\mu/V_2=0.5$ indicated in the figure shows that it decreases the stacking-faulted substratum region to about 1/20 of the normal one; we notice that the transition temperature is lowered to some

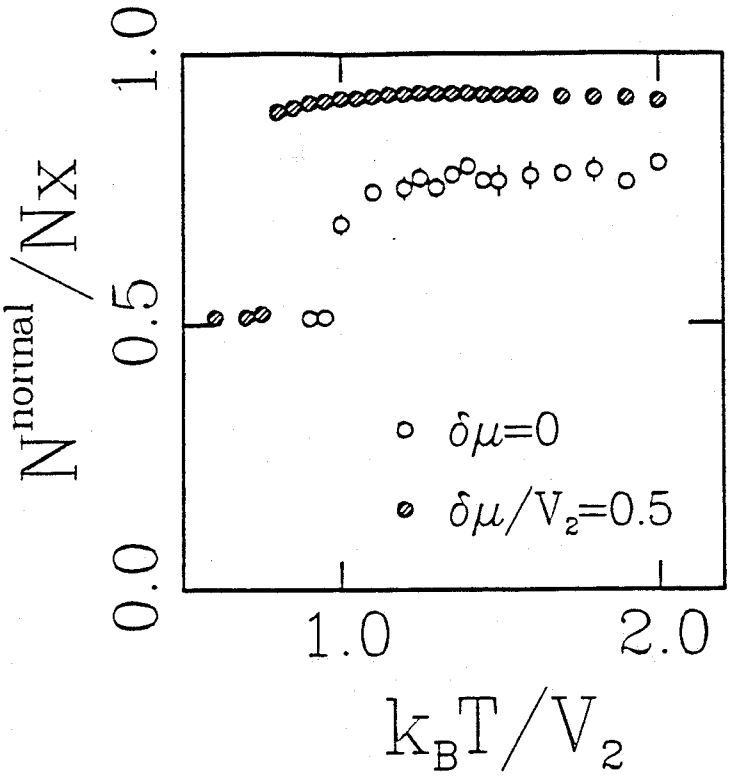

Figure 4.7
Temperature dependence of the number of particles corresponding to adatoms on the normal substratum layer. Open and hatched circles correspond to the cases of $\delta\mu/V_2$=0 and 0.5, respectively.

extent by finite $\delta\mu$, as we expect, but that the ordered state is still the (7×7) one. The present result justifies the simple lattice gas model for the (1×1) phase of the Si(111) surface.

CHAPTER V

Summary and Discussion

In this chapter we present a brief summary of the results obtained in the previous chapters, Chaps. III and IV, and some additional discussions of the present investigation.

§5.1 Summary

We have carried out the Monte Carlo calculation of two lattice gas models which reproduce well the temperature dependence of Ge(111) and Si(111), respectively, both below and above the transition.

In the investigation on the Ge(111) surface phase diagrams and diffuse scatterings of electron in the high-temperature (1×1) phase within the kinematical approximation have been presented, carrying out Monte Carlo calculations of the simple lattice gas model with up to the sixth neighbour interaction on a triangular net. The phase transition from each of the ordered states, the (2×2), c(2×4), and c(2×8) ones, into the (1×1) has been shown to be of the first kind. It has been shown that the temperature dependence of diffuse scatterings observed in the RHEED and LEED experiments can be reproduced by the model. The origin of the temperature evolution of the characteristic diffuse patterns has

been discussed on the basis of the calculations. We have found that in a temperature range above the transition the (1×1) state following the c(2×8) ordered one is divided into domains of irregular polygons in each of which particles take a (2×2) arrangement; the domain structure reproduces the characteristic diffuse scattering observed in the experiments. The underlying mechanism of the characteristic domain structure of particle arrangements just above the transition has also been discussed.

In the investigation on the Si(111) surface we have proposed an extended lattice gas model where the Takayanagi mechanism stabilizing the (7×7) arrangement of adatoms is incorporated. It has been shown that the model transforms from the (7×7) state into the (1×1) one; the phase transition is of the first kind which is in agreement with experiments. We have also shown that the diffuse scatterings of electron in the (1×1) phase observed in the LEED and RHEED experiments can be reproduced by the model. Moreover, we have demonstrated that the stacking faults should decrease in the (1×1) phase even when we do not assign any additional energy to them; the entropy increase causes the decrease, because the Takayanagi wall hinders random distributions of adatoms. In addition, with the finite energy increase by yielding a stacking fault a more distinct decrease of stacking faults in the (1×1) phase has been shown. From the calculations, we have concluded the disappearance of the stacking fault in the (1×1) phase of the Si(111) surface.

§5.2 Supplementary Discussions

Before closing the present thesis, we give several additional discussions associated with the (111) surfaces of Si and Ge and the lattice gas model. We discuss first that we can understand the reconstruction of Si(111) and Ge(111) in a unified way with the lattice gas model. In §§5.2.2, §§5.2.3, and §§5.2.4, some discussions about the (1×1) phases of Ge(111) and Si(111) which supplement the discussion in Chaps. III and IV are presented. In §§5.2.5 the possibility of the floating phase in the lattice gas model is discussed. Finally in §§5.2.6 a supplementary description of the lattice gas models with which we have made an investigation on the surface problems is presented.

§§5.2.1 *A Unified Understanding of the Reconstruction of Si(111) and Ge(111)*

As is shown in Chap. III, the simple lattice gas model can reproduce features of the Ge(111) surface in the whole temperature range both below and above the transition. Moreover, the (1×1) phase of the Si(111) surface can be interpreted to correspond to the state of the model at temperatures high sufficiently to yield the strong $(\sqrt{3} \times \sqrt{3})$ short-range order. On the other hand, we have shown in Chap. IV that the extended lattice gas model is applicable to the Si(111) surface both below and above the transition. The simple lattice gas model is a specific case of the extended one. In Chap. IV we have assumed up to the third neighbour interaction between particles. If we add the repulsive sixth neighbour interaction, we can change a part of the param-

eter region where the ground state is the (2×2) state in the case with up to the third neighbour interaction into the region where the ground state is the c(2×8) one. Although we have a degree of freedom of orientations of a triangle in the extended model, a state just above the transition should be the one in the simple lattice gas model if we assume the sufficiently large value of $\bar{V}_2$. Thus we can describe the reconstruction of Ge(111) in the whole temperature range with the lattice gas model applicable to Si(111).

The difference of the constituents of the surfaces is probably reflected in the effective interaction between adatoms. Thereby the difference between the ordered structures of the surfaces is produced. In both the (1×1) phases of the surfaces, triplets of mutually second neighbouring particles which give the entropy gain necessary in the (1×1) phase play the primary role in the reconstrutions. It seems that more entropy is necessary for the (1×1) state of Si(111) than that of Ge(111) because of the more stability of the ordered state due to the Takayanagi mechanism. This gives the difference between the (1×1) states of the surfaces.

Finally, we notice that the lattice gas model is probably applicable to such systems as the Ge(111)-Sn surface, the Si(111)-Ge one, and the C(111) one which show the reconstruction similar to that of the (111) surfaces of Si and Ge.

§§5.2.2 *Additional Discussion on the (1×1) Phase of Ge(111)*

In §§3.5.1 we have calculated the temperature evolution of the grobal correlation function in the reciprocal space and shown that the qualitative feature which is observed in the diffraction ex-

periments of electron on the Ge(111) surface can be reproduced for any sets of interaction parameters with which the c(2×8) state is the ordered state. For quantitative comparison, however, it is necessary to adjust the interaction parameters; in the subsection we have demonstrated that the temperature dependence of the splitting of diffuse peaks around the (2×2) superlattice Bragg points can be well reproduced by the present lattice gas model, having a choice of the parameter set.

In another feature of the diffuse peaks we have a discrepancy between the LEED and RHEED experiments (Ichikawa and Ino, 1980; Phaneuf and Webb, 1985); the peak width in the RHEED experiment is smaller than that in the LEED one. Therefore we have not presented the comparison of the calculated temperature dependence of the peak width with the experiments. We believe, however, we can also show that the present model quantitatively well reproduces the temperature dependence of the peak width observed in experiments, if we have the more settled experimental data.

Detailed experimental data for the temperature dependence of the peak height of the diffuse spots have not been reported as yet. When we have the experimental data, we shall be able to show the present model to reproduce it also.

§§5.2.3 *Dependence of Adatom Concentration on Temperature*

Although the concentration of particles has been fixed in a value near 1/4 in the calculation for Ge(111), in practice the number of adatoms on the surface might be changed with tem-

perature. Now we have no experimental data on the temperature dependence of the concentration of adatoms. With the experimental data, however, we could show that the present lattice gas model reproduce the temperature evolution of the surface; then it would be necessary to choose another set of the interaction parameters appropriate for the case.

We notice a recent experimental work by medium-energy ion scattering (van der Gon *et al.*, 1991). From the comparison of the experiment with a computer simulation of the ion scattering experiment, they have concluded the reduction of the adatom concentration above the transition to about 60% of the concentration in the ordered state. With a reason of the large reduction of adatom concentration, one may have an impression that our treatment with the lattice gas model fixing the particle concentration at 1/4, i.e., the value in the ordered state is not fit for the discussion of the reconstruction of Ge(111) in the (1×1) phase. Their conclusion is, however, just an interpretation of the result of the experiment on the basis of a simulation performed by them; another interpretation of the experimental data may be effective. Moreover, the concluded value of the concentration of adatoms above the transition seems to be strongly dependent on the energy of incident ion beam; it is distributed from 50% to 75% within the incident energies adopted in their experiment. Thus we cannot ask at this stage only from the experiment whether or not the present investigation with fixing the particle concentration at 1/4 misfits the problem of the reconstruction of the surface; we stress that the present model reproduces features of the surface successfully.

§§5.2.4 *Additional Discussion on the (1×1) Phase of Si(111)*

In the LEED experiment on the (1×1) phase of the Si(111) surface additional diffuse spots at the (2×2) superlattice Bragg points are observed along with the diffuse ones around the ($\sqrt{3} \times \sqrt{3}$) superlattice Bragg points (Iwasaki *et al.*, 1987). As is shown in Fig. 4.6, the feature can be reproduced by the present lattice gas model. However, the (2×2) diffuse spots there split into two; the splitting of the spots is disagreement with the experiment. The direction towards which the spots split corresponds to the division into domains by such a network of walls as in the (7×7) ordered state but unlike that seen in the (1×1) state of the simple model applicable to Ge(111). In the present thesis we give no reason with which the additional diffuse spots are caused. It is left for the future to clarify the feature in the experiment.

It has also been reported that the slight displacement from the ($\sqrt{3} \times \sqrt{3}$) positions of the diffuse spots around the ($\sqrt{3} \times \sqrt{3}$) superlattice Bragg points are observed and that the spots show the threefold symmetry and rotate around the ($\sqrt{3} \times \sqrt{3}$) superlattice Bragg points with the change in the primary energy of electron (Iwasaki *et al.*, 1987). These features cannot be reproduced within the present treatment with the lattice gas model on a triangular net, since the model possesses the full symmetry of the triangular lattice, i.e., the sixfold symmetry. If we would like to reproduce them, we just try to extend the model into one on a honeycomb lattice where the two triangular sublattices are distinguished between.

§§5.2.5 *Floating Phase*

Kanamori previously conjectured (Kanamori and Okamoto, 1985; Kanamori, 1986) that the (1×1) phase of Ge(111) might correspond to the floating phase (Nelson and Halperin, 1979) which is discussed by Villain and Bak (1981) for the case of the axial next-nearest neighbour Ising (ANNNI) model (Elliott, 1961; Fisher and Selke, 1980). In the present lattice gas model the floating phase may appear between the ordered c(2×8) phase and the disordered (1×1) one if we choose the parameter set within a region in the parameter space very close to the (2×2) region. The transition temperatures around the phase boundary between the (2×2) and c(2×8) ordered phases are relatively high, as has been shown in the calculated phase diagram Fig. 3.8; this shows that the discommensuration walls are still stable at relatively high temperatures. In fact in the present Monte Carlo calculations for the wall energy $w \approx 0$ the state where ν walls with $\nu < L/4$ (ν=$L/4$ corresponds to the c(2×8) state) run parallel has been observed at temperatures around the transition, though the meandering of the walls with kinks for which it is necessary to decrease the number of particles does not take place because of the assumption that the concentration of particles is fixed at 1/4. This state, however, appears within a very small region of the interaction parameter space, while the polygonal domain structure which has been found in the present investigation is the general feature in the (1×1) phase of the present lattice gas model whose ordered state is the c(2×8). Therefore it is natural to conclude that the domain structure found

in the present Monte Carlo study corresponds to the (1×1) state of the Ge(111) surface; the state divided by (2×2) domains can be considered to be a substitute for the floating state which produces the characteristic diffuse spots in the reciprocal-space correlation function. Nevertheless, it is quite interesting from the statistical-mechanical point of view to confirm the appearance of the floating phase in a model with the isotropic interaction unlike the case of the ANNNI model. It is reported that the eighth-order spots move towards the (2×2) superlattice Bragg points with temperature between the c(2×8) state and the (1×1) one. The floating state in the present model may give an explanation of the aspect.

§§5.2.6 *Supplementary Discussion of the Models*

We have presented the Monte Carlo calculation of the two lattice gas models on a triangular net which, we believe, elucidates the underlying mechanism of the phase transition and the temperature evolution of the short-range order in the (1×1) phase. One may have the impression that the lattice gas models assume too much details of the interaction. We emphasize here that the essential mechanisms deduced from the calculation can be given in general terms, although one has to return to a well defined model for quantitative details. In other words, the assumed particular interactions in the models are the simplest representatives of those capable of explaining the interrelations among the experimental results which have not been elucidated so far.

We discuss first the case of Ge(111) for which the simple lattice gas model is shown to be applicable. The ordered struc-

ture can be discussed in terms of the energy required to produce a discommensuration wall in the (2×2) state, the interaction energy between adjacent walls, and the energy of the intersection of the walls, provided that the interaction of the nearest neighbouring pairs of particles on the triangular lattice is repulsive enough to forbid the formation of them. If the wall interaction unfavours the smallest interval of the walls and the wall intersection energy is sufficiently positive, the c(2×8) state is realized as the ground state; at the same time the (7×7) state of this simple lattice gas is proved not to be the ground state. The sixth neighbour interaction invoked in the present model is the interaction of the shortest distance which is capable of producing the wall interaction. The physical mechanism underlying the wall interaction may be an elastic energy produced by accompanying elastic strains of adatoms which may give rise to more distant neighbour interactions than sixth as well. We emphasize that the most essential part of the wall interaction is the energy difference between the shortest interval and larger intervals which the sixth neighbour interaction is capable of representing. We have shown that the interaction produces the uniformity of the domain sizes in the (1×1) phase just above the transition temperature which explains the sharpness, approximate positions, and direction of the temperature evolution of diffuse spots. Thus we assert that our statistical-mechanical approach has elucidated the essential mechanism operating in the Ge(111) surface for the evolution of the reconstructed structure in the whole temperature range.

In the case of Si(111) we have extended the model to in-

corporate the possibility of a lower energy of the wall of the Takayanagi model which separates the stacking faulted substratum from the normal substratum. With this device we can stabilize the (7×7) state as the ground state. Takayanagi and Tanishiro (1986) previously proposed a similar model to the present one; by the use of it they discussed the DAS structures corresponding to the (7×7) state of Si(111) and the c(2×8) one of Ge(111). The DAS structure of c(2×8) state they proposed is the same one proposed by Kanamori (1986) independently; we notice that the structure model for Ge(111) is now being settled negatively. We stress here that the present model is one defined completely as a lattice gas model with extended range pairwise interactions for the purpose of discussing the reconstruction of the (111) surface of Si at finite temperatures.

Acknowledgements

I would like to express my sincere thanks to Professor Junjiro Kanamori for his introducing me into the investigation on the surface problem, his helpful discussions with me, and his critical reading of the manuscript of the thesis.

I would also like to record my warmest acknowledgements to Dr. Macoto Kikuchi for many valuable discussions and his guidance in the Monte Carlo calculation.

Last but not least, I would like to thank to Professors J. Kanamori, K. Murase, H. Ohtsubo, T. Jo, and Y. Akutsu for their troubling themselves to hold an inquiry into the present thesis.

References

Aarts, J., A.-J. Hoeven, and P. K. Larsen, 1988, Phys. Rev. B**38**, 3925.

Bak, P., D. Mukamel, J. Villain, and K. Wentowska, 1979, Phys. Rev. B**19**, 1610.

Baxter, R. J., 1980, J. Phys. A**13**, L61.

Becker, R. S., J. A. Golovchenko, and B. S. Swartzentruber, 1986, Phys. Rev. Lett. **57**, 1020.

Becker, R. S., B. S. Swartzentruber, J. S. Vickers, and T. Klitsner, 1989, Phys. Rev. B**39**, 1633.

Binder, K., 1981, Z. Phys. B**45**, 61.

Binnig, G., H. Rohrer, Ch. Gerber, and E. Weibel, 1983, Phys. Rev. Lett. **50**, 120.

Chadi, D. J., and T.-C. Chiang, 1981, Phys. Rev. B**23**, 1843.

Domany, E., M. Schick, and J. S. Walker, 1977, Phys. Rev. Lett. **38**, 1148.

Domany, E., M. Schick, J. S. Walker, and R. B. Griffiths, 1978, Phys. Rev. B**18**, 2209.

Elliott, R. J., 1961, Phys. Rev. **124**, 346.

Feidenhans'l, R., J. S. Pedersen, J. Bohr, M. Nielsen, F. Grey, and R. L. Johnson, 1988, Phys. Rev. B**38**, 9715.

Fisher, M. E., and W. Selke, 1980, Phys. Rev. Lett. **44**, 1502.

Fujimoto, M., *unpublished.*

van der Gon, A. W. D., J. M. Gay, J. W. M. Frenken, and J. F. van der Veen, 1991, Surf. Sci., *in press.*

Henzler, M., 1969, J. Appl. Phys. **40**, 3758.

Ichikawa, T., and S. Ino, 1980, Solid State Commun. **34**, 349.

Ino, S., 1977, Jpn. J. Appl. Phys. **16**, 891.

Iwasaki, H., S. Hasegawa, M. Akizuki, S.-T. Li, S. Nakamura, and J. Kanamori, 1987, J. Phys. Soc. Jpn. **56** 3425.

Kaburagi, M., and J. Kanamori, 1974, Jpn. J. Appl. Phys. Suppl. 2, Pt.2, 145.

Kaburagi, M., and J. Kanamori, 1975, Prog. Theor. Phys. **54**, 30.

Kaburagi, M., and J. Kanamori, 1978, J. Phys. Soc. Jpn. **44**, 718.

Kanamori, J., 1966, Prog. Theor. Phys. **35**, 16.

Kanamori, J., 1984, Solid State Commun. **50**, 363.

Kanamori, J., 1985, Ann. Phys. Fr. **10**, 43.

Kanamori, J., 1986, J. Phys. Soc. Jpn. **55**, 2723.

Kanamori, J., and M. Okamoto, 1985, J. Phys. Soc. Jpn. **54**, 4636.

Kanamori, J., and Y. Sakamoto, 1991, Surf. Sci., Proc. of The 26th Yamada Conf., July 2-6, 1990, Osaka, Japan. *in press.*

Kirkpatrick, S., and E. P. Stoll, 1981, J. Comput. Phys. **40**, 517.

Lander, J. J., 1964, Surf. Sci. **1**, 125.

Lewis, T. G., and W. H. Payne, 1973, J. Assoc. Comput. Mach. **20**, 456.

Marée, P. M. J., K. Nakagawa, J. F. van der Veen, and R. M. Tromp, 1988, Phys. Rev. B**38**, 1585.

Metropolis, N., A. W. Rosenbluth, M. N. Rosenbluth, A. H. Teller, and E. Teller, 1953, J. Chem. Phys. **21**, 1087.

Nelson, D. R., and B. I. Halperin, 1979, Phys. Rev. B**19**, 2457.

Palmberg, P. W., and W. T. Peria, 1967, Surf. Sci. **6**, 57.

Palmberg, P. W., 1968, Surf. Sci. **11**, 153.

Phaneuf, R. J., and M. B. Webb, 1985, Surf. Sci. **164**, 167.

Sakamoto, Y., and J. Kanamori, 1989a, J. Phys. Soc. Jpn. **58**, 1512.

Sakamoto, Y., and J. Kanamori, 1989b, J. Phys. Soc. Jpn. **58**, 2083.

Sakamoto, Y., and J. Kanamori, 1991, Surf. Sci., Proc. of The 26th Yamada Conf., July 2-6, 1990, Osaka, Japan. *in press.*

Schlier, R. E., and H. E. Farnsworth, 1959, J. Chem. Phys. **30**, 917.

Takayanagi, K., Y. Tanishiro, M. Takahashi, and S. Takahashi, 1985, J. Vac. Sci. Technol. A**3**, 1502.

Takayanagi, K., and Y. Tanishiro, 1986, Phys. Rev. B**34**, 1034.

Tausworthe, R. C., 1965, Math. Comput. **19**, 201.

Villain, J., and P. Bak, 1981, J. Phys. (France) **42**, 657.

Yang, W. S., and F. Jona, 1984, Phys. Rev. B**29**, 899.